ISSN 1064-2269, Journal of Communications Technology and Electronics, 2016, Vol. 61, No. 6, pp. 551–573. © Pleiades Publishing, Inc., 2016.
Original Russian Text © V.Yu. Shishkov, A.A. Zyablovskii, E.S. Andrianov, A.A. Pukhov, A.P. Vinogradov, A.V. Dorofeenko, S.A. Nikitov, A.A. Lisyanskii, 2016, published in Radiotekhnika i Elektronika, 2016, Vol. 61, No. 6, pp. 509–533.

REVIEW

Wide-Aperture Planar Lasers

V. Yu. Shishkov[a, b], A. A. Zyablovskii[a, b], E. S. Andrianov[a, b], A. A. Pukhov[a, b, c], A. P. Vinogradov[a, b, c], A. V. Dorofeenko[a, b, c], S. A. Nikitov[a, d], and A. A. Lisyanskii[e, f]

[a] *Dukhov All-Russia Research Institute of Automatics, Sushchevskaya ul. 22, Moscow, 127055 Russia*
[b] *Moscow Institute of Physics and Technology (State University), Institutskii per. 9, Dolgoprudnyi, Moscow oblast, 141700 Russia*
[c] *Institute for Theoretical and Applied Electrodynamics, Russian Academy of Sciences, Izhorskaya ul. 13, Moscow, 125412 Russia*
[d] *Kotel'nikov Institute of Radio Engineering and Electronics, Russian Academy of Sciences, Mokhovaya ul. 11, str. 7, Moscow, 125009 Russia*
[e] *Queens College, The City University of New York, 65-30 Kissena Blvd., Queens, NY 11367-1597 USA*
[f] *The Graduate Center, The City University of New York, 365 Fifth Avenue, New York, NY 10016 USA*
e-mail: zyablovskiy@mail.ru

Received January 27, 2015

Abstract—Wide-aperture planar lasers (vertical-cavity surface emitting lasers, distributed feedback lasers, 2D spaser arrays, and plasmon lasers on stopped-light mode) are reviewed. Structure, parameters (directional pattern and amplitude modulation frequency), and physical principles of such lasers are discussed.

DOI: 10.1134/S1064226916050107

INTRODUCTION

The development of communication technologies necessitates the construction of devices for conversion of electrical signals into optical signals for the transmission in optical communication channels. The following requirements must be satisfied for such devices: relatively high modulation frequency of signals, low generation threshold, narrow directional pattern of output signal, and low production costs. Lasers with cavities based on a defect mode in photonic crystal (vertical-cavity surface emitting (VCSE) lasers) [1–4] and distributed-feedback (DFB) lasers are used at present for such purposes. Sources of coherent radiation based on composite materials containing plasmon nanostructures [5–11] may serve as alternative sources. The modulation frequency that is higher than that of the VCSE and DFB lasers is the main advantage of the alternative sources.

Normally, a VCSE laser consists of two 1D photonic crystals[1] (Bragg mirrors) with a resonant cavity in between [12–20] and amplifying medium that is placed in the resonant cavity. The laser generation in such devices takes place along the direction that is perpendicular to the layer plane.

The amplifying medium in a VCSE laser represents a thin layer of a narrow-band-gap semiconductor that is placed between two layers of a wide-band-gap semiconductor. Such a heterostructure works as a quantum well when the amplifying layer is relatively thin [12]. The total energy of carriers in quantum wells is a sum of discrete levels that emerge owing to the space quantization along the direction that is perpendicular to the layer and a continuous component that describes the motion along the layer:

$$E_{\text{tot}} = \frac{p^2}{2m} + \frac{\pi^2\hbar^2}{2ml^2}n^2, \quad (1)$$

where p are the momenta of carrier along the layer, m is the effective mass of carrier, l is the layer thickness, and n is the integer.

Radiative transitions of electron from the conduction band to the valence band serve as working levels in quantum wells. The photon frequency in quantum wells is a sum of the band gap of bulk semiconductor and a discrete quantity related to the finite thickness of the semiconductor film. The dependence of the transition frequency on the film thickness can be used to accurately tune the transition frequency to the cavity mode [12].

When the thickness of the resonant cavity is one half of the wavelength of the generated radiation, the single-mode lasing is easily reached in VCSE lasers [17, 21]. The VCSE laser can be stabilized with respect to thermal fluctuations owing to a relatively high Q factor of the vertical cavity. The amplification band is highly sensitive to the thermal fluctuations [15].[2] If the

[1] See Appendix 1 for the properties of photonic crystals.

[2] Temperature variations lead to variations in the thickness of layers in the VCSE-laser structure, so that the mode frequency of the cavity and frequency of amplification band are varied. The frequency of cavity mode is inversely proportional to the layer thickness, and the frequency of the amplification band is inversely proportional to the squared thickness owing to space quantization of the energy of carriers. Therefore, the frequency of the amplification band is significantly more sensitive to variations in temperature in comparison with the frequency of the cavity mode.

amplification band is significantly broader than the cavity band, the latter determines the laser frequency (frequency pulling) [12, 22, 23]. Such a frequency stability is an advantage of vertical-cavity lasers in optoelectronic applications in which the laser frequency must be tuned to the waveguide mode of optical fiber.

A DFB laser may serve as an alternative to a VCSE laser. In the DFB lasers, the laser mode is generated owing to multiple scattering by periodic photonic-crystal structure rather than reflection from cavity mirrors.

The DFB lasers that are employed in optoelectronics contain plates of 2D photonic crystal (PC) in which amplifying medium is used as a matrix [24]. The wave vector of the laser mode in such systems belongs to the plate plane and the generated radiation is emitted along the perpendicular direction.[3] The emission from the PC surface takes place due to the fact that the spatial spectrum of the Bloch wave contains wave numbers the tangential components of which are less than the wave number in surrounding space. The width of the directional pattern of the emitter is determined by the size of the emitting aperture, in particular, the transverse size of the PC plate. Therefore, the size of the PC plate must be significantly greater than the wavelength.[4] An increase in the PC size leads to a decrease in loss related to the emission from the end surfaces of the plate and, hence, a decrease in the lasing threshold.

Note the nonlinearity of the regime of developed generation. In this case, the permittivity of the active matrix depends on the field intensity and is modulated with the period of the Bloch wave. In general, the period of the Bloch wave is incommensurable with the PC period and the development of lasing causes distortions of the PC periodicity. Thus, the mode ceases to be the mode of the Bloch wave, the scattering by single cells looses long-range order, and the directional pattern becomes broader. In the exceptional case, the lasing in the DFB laser takes place at frequencies in the vicinity of the boundary of the PC band gap, so that the period of the Bloch wave almost coincides with the PC period and the modulation of the active medium caused by the generated wave does not lead to violations of the PC periodicity.

The closeness of the laser frequency to the edge of the band gap determines the physical scenario of lasing. Owing to the Bragg reflection, the Bloch wave at the edge of the band gap is transformed into a standing wave, so that the conditions for the cavityless lasing are satisfied. This circumstance accounts for the term distributed-feedback lasers.

[3] In the first DFB lasers, the radiation was emitted along the direction of generation. However, such a configuration cannot be used to construct a radiation source with a relatively narrow directional pattern.

[4] A narrow beam is needed for efficient delivery of the optical signal of the DFB laser to optical fiber.

Thus, the modes at the boundary of the PC band gap exhibit the lowest lasing threshold, the radiation of such modes is emitted along the direction that is orthogonal to the plane of the PC plate, and the development of lasing at frequencies in the vicinity of the boundary of the PC band gap does not destroy the PC periodicity.

1. SIMPLIFIED MODEL OF DFB LASER

To illustrate the above analysis, we consider a DFB laser (Fig. 1). We assume that the plate made of the amplifying medium is placed in lossless medium with permittivity ε_{lm}.

To describe the interaction of electromagnetic field and amplifying medium, we use the system of the Maxwell–Bloch equations [25] that is represented in the following way for the propagation along the direction that is perpendicular to layers [25, 26]:

$$\frac{\partial^2 E}{\partial x^2} - \frac{\varepsilon(x)}{c^2}\frac{\partial^2 E}{\partial t^2} = \frac{4\pi}{c^2}\frac{\partial^2 P}{\partial t^2}, \tag{2}$$

$$\frac{\partial^2 P}{\partial t^2} + \frac{2}{\tau_p}\frac{\partial P}{\partial t} + \omega_{QD}^2 P = -\frac{2\omega_{QD}\left|\vec{d}\right|^2 nE}{\hbar}, \tag{3}$$

$$\frac{\partial n}{\partial t} + \frac{1}{\tau_{inv}}(n - n_0) = \frac{2}{\hbar\omega_{QD}} E\frac{\partial P}{\partial t}. \tag{4}$$

Here, E is the electric field, P is the polarization, n is the population inversion of the gain medium, n_0 is the population inversion that is reached in the medium in the absence of electromagnetic field, ω_{QD} is the transition frequency of quantum dots (QDs), $\left|\vec{d}\right|^2$ is the square of the dipole moment of the transition in the gain medium, and τ_p and τ_{inv} are the characteristic relaxation times of polarization and population inversion. The system of the Maxwell–Bloch equations was derived in [25] on the assumption that the amplifying medium represents an ensemble of two-level systems the population inversion in which results from external action. The two-level systems were described using the quantum-mechanical equations for the density matrix that are reduced to equations for polarization P and population inversion n. The electromagnetic field in the system was analyzed on the assumption that quantum fluctuations can be disregarded owing to a relatively large number of photons in the system and that the field can be described with the aid of classical Maxwell equations. The field amplification results from the stimulated transitions in the amplifying medium, and the energy transition from the amplifying medium to the electromagnetic wave is described using a term on the right-hand side of Eq. (2). Such an approximation is known as the semiclassical approximation [25].

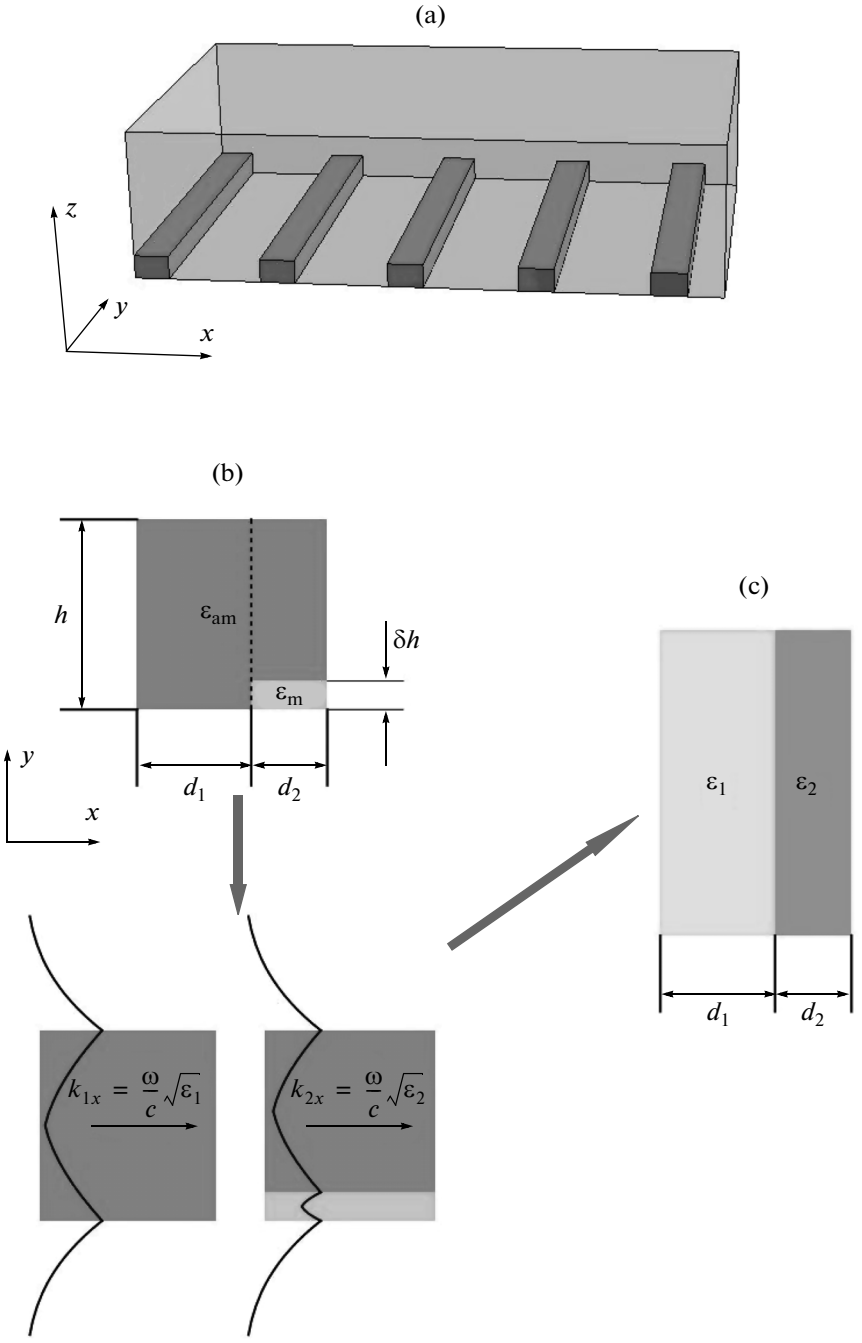

Fig. 1. (a) Scheme of the DFB laser consisting of an amplifying layer that contains a periodic grating of nanoribbons, (b) scheme of a unit cell of the DFB laser, and (c) a cell of an auxiliary 1D PC with effective permittivities of layers ε_1 and ε_2.

Maxwell–Bloch equations (2)–(4) make it possible to describe the interaction of electromagnetic field and amplifying medium. For relatively low fields $\left(\left|n - n_0\right| = \frac{2\tau_{inv}}{\hbar\omega_{QD}}\left|E\frac{\partial P}{\partial t}\right| \ll n_0\right)$, population inversion is virtually constant and field-independent. In this case, the field and polarization can be analyzed using linear equations (2)–(4) and the amplifying medium can be described with the aid of permittivity with negative frequency-dependent imaginary part:

$$\varepsilon_{am}(\omega) = \varepsilon_{pl} - \frac{2\alpha\omega_{QD}/\tau_p}{-2i\omega/\tau_p + \omega_{QD}^2 - \omega^2}, \quad (5)$$

where ε_{pl} is the permittivity of the plate in the absence of the amplifying medium, $\alpha = 4\pi\left|\vec{d}\right|^2\tau_p n_0/\hbar$, and $\beta =$

$\left|\vec{d}\right|^2 \tau_{inv}\tau_p/\hbar^2$ [26, 27], and ε_{am} is the permittivity of the amplifying medium that is used to fabricate the PC plate.

A periodic structure of nanoribbons (Fig. 1a) with permittivity ε_m is introduced into the film to produce the distributed feedback in the DFB laser. Film thickness is h, the distance between nanoribbons is d_1, the width of nanoribbon is d_2, and the height of nanoribbon is δh (Fig. 1b). The lower surface of the film lies on the xy plane.

A waveguide mode that is scattered by nanoribbons may propagate inside the film. The system under study is periodic along the x direction, and its single cell consists of two sections (Fig. 1b). The first section represents a homogeneous dielectric waveguide with thickness h and permittivity ε_{am} that is placed into medium with permittivity ε_{lm}. The second section is the homogeneous (with respect to the x axis) two-layer waveguide consisting of the layer with thickness $h - \delta h$ with permittivity ε_{am} and the layer with thickness δh and permittivity ε_m that is placed into medium with permittivity ε_{lm}. Such a system can be analyzed using an auxiliary 1D PC the single cell of which consists of two layers with effective permittivities ε_1 and ε_2 (Fig. 1c). The effective permittivity and impedance of the ith layer ($i = 1, 2$) can be calculated as $\varepsilon_i = c^2 k_{ix}^2/\omega^2$ and $Z_i = \sqrt{\varepsilon_i}$, where $k_{ix}(\omega)$ is the wave vector of the TE-polarized wave that propagates along the ith section of the waveguide (Fig. 1b).[5]

To find quantity $k_{2x}(\omega)$, we solve the boundary eigenvalue problem. The distributions of the electric and magnetic fields in the waveguide (Fig. 1b) are given by

$$E_y = \begin{cases} e^{ik_{2x}x+\gamma_{lm}z}, & z \le 0, \\ e^{ik_{2x}x}\left(a_{mode}e^{\gamma_{mode}z} + b_{mode}e^{-\gamma_{mode}z}\right), & z \in (0, \delta h), \\ e^{ik_{2x}x}\left(a_{am}e^{i\gamma_{am}z} + b_{am}e^{-i\gamma_{am}z}\right), & z \in [\delta h, h), \\ b_{lm}e^{ik_{2x}x-\gamma_{lm}z}, & z \ge h \end{cases} \quad (6)$$

$$H_x = \partial E_y/\partial z,$$

where k_{2x} is the wave number along the waveguide axis,

$$\gamma_{lm} = \sqrt{k_{2x}^2 - \left(\frac{\omega}{c}\right)^2 \varepsilon_{lm}}, \quad \gamma_{mode} = \sqrt{k_{2x}^2 - \left(\frac{\omega}{c}\right)^2 \varepsilon_{mode}},$$

$$\gamma_{am} = \sqrt{\left(\frac{\omega}{c}\right)^2 \varepsilon_{am} - k_{2x}^2}$$

are the wave numbers along the z axis in the external medium, nanoribbon of the auxiliary waveguide, and active medium of the auxiliary waveguide, respectively. Amplitudes, a_{mode}, b_{mode}, a_{am}, b_{am}, and b_{lm} are found from the boundary conditions at the edges of layers. With allowance for the boundary conditions, the dispersion relation for wave vector $k_{2x}(\omega)$ is written as

$$\begin{aligned} &\gamma_{am}\left(\gamma_{am}\sin\left(\gamma_{am}(h-\delta h)\right) - \gamma_{lm}\cos\left(\gamma_{am}(h-\delta h)\right)\right) \\ &\quad\times\left(\gamma_{lm}\sinh\left(\gamma_{mode}\delta h\right) + \gamma_{mode}\cosh\left(\gamma_{mode}\delta h\right)\right) \\ &\qquad= \gamma_{mode}\left(\gamma_{am}\cos\left(\gamma_{am}(h-\delta h)\right)\right. \\ &\qquad\quad\left. - \gamma_{lm}\sin\left(\gamma_{am}(h-\delta h)\right)\right) \\ &\quad\times\left(\gamma_{lm}\cosh\left(\gamma_{mode}\delta h\right) + \gamma_{mode}\sinh\left(\gamma_{mode}\delta h\right)\right). \end{aligned} \quad (7)$$

We must assume that $\delta h = 0$ in expression (7) to calculate wave vector $k_{1x}(\omega)$ at the fragment of the waveguide outside the nanoribbon. In calculations, we use parameters ε_{lm}, ε_{am}, ε_{mode}, h, and δh from experiments on DFB lasers [9, 28] and obtain $\mathrm{Re}\,\varepsilon_1 = 1.5$, $\mathrm{Re}\,\varepsilon_2 = 1.1$, and imaginary parts of ε_1 and ε_2 that do not depend on the pump intensity. Below, we study the working regimes of the DFB laser at different $\mathrm{Im}\,\varepsilon_1$ and $\mathrm{Im}\,\varepsilon_2$.

The properties of 1D PC are well known (see Appendix 1). The lasing threshold in PC is determined by the condition [26, 29]

$$r^2\exp(2ik_B Nd) = 1, \quad (8)$$

where N is the number of PC cells, d is the length of the PC cell, r is the reflection coefficient for the PC–vacuum interface, and k_B is the Bloch wave number in the PC. Expression (8) can be divided into amplitude and phase conditions for lasing. The amplitude condition

$$\mathrm{Im}\,k_B(n_0)d = \frac{\ln|r|}{N}. \quad (9)$$

Makes it possible to determine the minimum population inversion n_0 that is needed for lasing. Note that Bloch wave vector $k_B(n_0)$ depends on the permittivity of active layers that, in turn, nonlinearly depends on population inversion n_0. In the DFB laser, the reflection from the end surfaces of the plate is insignificant, since the standing mode emerges in the system due to multiple scattering by the PC periodic structure. Indeed, an increase in the number of the PC cells always leads to the scenario in which $N \gg \ln|r|$, so that the loss related to the emission from the end surfaces of the PC can be neglected. In this case, expression (9) is reduced to equation

$$\mathrm{Im}\,k_B = 0. \quad (10)$$

In other words, the lasing threshold for the PC with $L \gg \lambda$ is determined only by the loss related to emission along the direction perpendicular to the PC plane

[5] Such a polarization configuration is chosen with allowance for the fact that the dipole moments of nanoribbons are induced by electric field, so that a narrow directional pattern with the maximum along the normal to the PC can be obtained only for the TE polarization.

and the internal loss in the PC-cell material. The condition $N \gg \ln|r|$ can easily be satisfied at the boundary of the band gap where the PC impedance is written as $Z_{PC} \approx iZ_{PC}$ (see Appendix 1), so that the absolute value of the reflection coefficient for the PC–insulator interface is represented as

$$|r| = \left|\frac{Z_{PC} - Z_{am}}{Z_{PC} + Z_{am}}\right| \approx 1.$$

Using expression (8), we derive the phase condition

$$\mathrm{Re}\, k_B(\omega) Nd + \arg(r) = \pi n, \tag{11}$$

where n is the integer. Expression (11) makes it possible to determine the radiation frequency of the DFB laser. It is seen that the lasing takes place when the phase shift related to a single passage through the system is a multiple of π.

At frequencies that are close to the second boundary of the band gap, we have $\mathrm{Re}\, k_B(\omega) = \frac{2\pi}{d} + \delta k(\omega)$, where $|\delta k(\omega)| \ll \frac{2\pi}{d}$. Using formula (11), we obtain

$$\delta k(\omega) = \frac{\pi m - \arg(r)}{L} \ll \frac{\pi}{d}, \tag{12}$$

where $m = n - N$. Note that $m = \pm 1$ for PC modes that are closest to the band gap.

To find threshold population inversion n_0^{thr} from expression (10), we must determine the dependence of quantity $\mathrm{Im}\, k_B(\omega)$ on the PC parameters with the aid of the Rytov equation [30] (see Appendix 1):

$$\mathrm{Im}\, k_B(\omega) = \frac{\mathrm{Im}\left(\arccos\left(\cos(k_1 d_1)\cos(k_2 d_2) - \frac{1}{2}\left(\frac{Z_1}{Z_2} + \frac{Z_2}{Z_1}\right)\sin(k_1 d_1)\sin(k_2 d_2)\right)\right)}{d_1 + d_2}. \tag{13}$$

Threshold parameter n_0^{thr} is implicitly determined using equation

$$\mathrm{Im}\left(\arccos\left(\cos(k_1 d_1)\cos(k_2 d_2) - \frac{1}{2}\left(\frac{Z_1}{Z_2} + \frac{Z_2}{Z_1}\right)\sin(k_1 d_1)\sin(k_2 d_2)\right)\right) = 0. \tag{14}$$

Expression (14) is an exact expression for the lasing threshold but, for estimations, we employ the system of Maxwell–Bloch equations (2)–(4). We assume that the lasing in the PC takes place in the vicinity of the QD transition frequency ω_{QD}. Then, electric field E and polarization P are represented as

$$E = e(x,t)\exp(i\omega_{QD}t) + e^*(x,t)\exp(-i\omega_{QD}t),$$
$$P = p(x,t)\exp(i\omega_{QD}t) + p^*(x,t)\exp(-i\omega_{QD}t),$$

where E and P are the real quantities and $e(x,t)$ and $p(x,t)$ are the complex functions the variations in which are substantially slower than variations in exponential function $\exp(i\omega_{QD}t)$. Using such a condition, we represent the Maxwell–Bloch equations as

$$\frac{\partial^2 e(x,t)}{\partial x^2} + \frac{\omega_{QD}^2}{c^2}\varepsilon(x)e(x,t) - i\frac{2\omega_{QD}\varepsilon}{c^2}\frac{\partial e(x,t)}{\partial t} = 4\pi\frac{\omega_{QD}^2}{c^2}p(x,t), \tag{15}$$

$$\frac{\partial p(x,t)}{\partial t} + \frac{p(x,t)}{\tau_p} = -\frac{i|\vec{d}|^2 ne(x,t)}{\hbar}, \tag{16}$$

$$\frac{\partial n(x,t)}{\partial t} + \frac{1}{\tau_{inv}}(n(x,t) - n_0) = \frac{4}{\hbar}\mathrm{Im}(e(x,t)p(x,t)). \tag{17}$$

At the initial stage of lasing, the population inversion is approximately n_0, since the field amplitude is insufficient for significant changes of the population inversion. In this case, nonlinear system of equations (15)–(17) is reduced to the linear system

$$\frac{\partial^2 e(x,t)}{\partial x^2} + \frac{\omega_{QD}^2}{c^2}\varepsilon(x)e(x,t) - i\frac{2\omega_{QD}\varepsilon}{c^2}\frac{\partial e(x,t)}{\partial t} = 4\pi\frac{\omega_{QD}^2}{c^2}p(x,t), \tag{18}$$

$$\frac{\partial p(x,t)}{\partial t} + \frac{p(x,t)}{\tau_{inv}} = -\frac{i|\vec{d}|^2 n_0 e(x,t)}{\hbar}. \tag{19}$$

Thus, slow amplitudes of the field and polarization can be represented as

$$e(x,t) = e_{mode}(x)a(t), \quad p(x,t) = e_{mode}(x)\sigma(t),$$

where function $e_{mode}(x)$ satisfies the equation

$$\frac{\partial^2 e_{mode}(x)}{\partial x^2} + \frac{\omega_{QD}^2}{c^2}\mathrm{Re}(\varepsilon(x))e_{mode}(x) = 0,$$

and, hence, serves as the mode of cavity that represents a finite sample of PC. Finally, we derive the following system of equations for variables $a(t)$ and $\sigma(t)$:

$$\frac{\partial a(t)}{\partial t}\varepsilon(x)e_{mode}(x) = -2\pi i\omega_{QD}\sigma(t)e_{mode}(x) + \mathrm{Im}(\varepsilon(x))\frac{\omega_{QD}}{2}a(t)e_{mode}(x), \tag{20}$$

$$\frac{\partial \sigma(t)}{\partial t}e_{mode}(x) = -\frac{1}{\tau_p}\sigma(t)e_{mode}(x) + i\frac{n_0}{\hbar}|\vec{d}|^2 a(t)e_{mode}(x). \tag{21}$$

We average spatial factors in expressions (20) and (21) with respect to the mode of the linear PC corresponding to frequency ω_{QD}:

$$\langle e_{mode}|f|e_{mode}\rangle = \frac{\int e^*_{mode}(x) f(x) e_{mode}(x)\,dx}{\int e^*_{mode}(x) e_{mode}(x)\,dx}.$$

Thus, we derive equations that make it possible to find functions $a(t)$ and $\sigma(t)$ with effective factors:

$$\frac{\partial a}{\partial t} = -\frac{2\pi i\omega_{QD}}{\langle e_{mode}|\varepsilon|e_{mode}\rangle}\sigma + \frac{\langle e_{mode}|\mathrm{Im}\,\varepsilon|e_{mode}\rangle}{\langle e_{mode}|\varepsilon|e_{mode}\rangle}\frac{\omega_{QD}}{2}a, \quad (22)$$

$$\frac{\partial \sigma}{\partial t} = -\frac{1}{\tau_p}\sigma + i\frac{|\vec{d}|^2}{\hbar}\langle e_{mode}|n_0|e_{mode}\rangle a. \quad (23)$$

The matrix representation of the system of equations (22) and (23) is

$$\frac{\partial}{\partial t}\begin{pmatrix} a \\ \sigma \end{pmatrix} = W\begin{pmatrix} a \\ \sigma \end{pmatrix}, \quad (24)$$

where

$$W = \begin{pmatrix} \omega_{QD}\langle e_{mode}|\mathrm{Im}\,\varepsilon|e_{mode}\rangle/(2\langle e_{mode}|\varepsilon|e_{mode}\rangle) & -2\pi i\omega_{QD}/\langle e_{mode}|\varepsilon|e_{mode}\rangle \\ i|\vec{d}|^2\langle e_{mode}|n_0|e_{mode}\rangle/\hbar & -1/\tau_p \end{pmatrix}.$$

The solution to Eq. (24) is written as

$$\begin{pmatrix} a \\ \sigma \end{pmatrix} = c_1\begin{pmatrix} a_1 \\ \sigma_1 \end{pmatrix}\exp(\lambda_1 t) + c_2\begin{pmatrix} a_2 \\ \sigma_2 \end{pmatrix}\exp(\lambda_2 t), \quad (25)$$

where (a_i, σ_i) and λ_i are eigenvectors and eigenvalues of matrix W, respectively, and c_i are the amplitudes of eigenvectors that depend on the initial conditions. If the real part of either eigenvalue is positive, the amplitude of the corresponding eigenvector of matrix W infinitely increases with time, which corresponds to the presence of lasing. The eigenvalues of matrix W are given by

$$\lambda_\pm = -\left(\frac{1}{\tau_p} + \frac{\omega_{QD}}{2}\frac{\langle e_{mode}|\mathrm{Im}\,\varepsilon|e_{mode}\rangle}{\langle e_{mode}|\varepsilon|e_{mode}\rangle}\right) \pm \sqrt{\left(\frac{1}{\tau_p} + \frac{\omega_{QD}}{2}\frac{\langle e_{mode}|\mathrm{Im}\,\varepsilon|e_{mode}\rangle}{\langle e_{mode}|\varepsilon|e_{mode}\rangle}\right)^2 - 4\left(\frac{\omega_0}{2\tau_p}\frac{\langle e_{mode}|\mathrm{Im}\,\varepsilon|e_{mode}\rangle}{\langle e_{mode}|\varepsilon|e_{mode}\rangle} - 2\pi\omega_{QD}|\vec{d}|^2\frac{\langle e_{mode}|n_0|e_{mode}\rangle}{\langle e_{mode}|\varepsilon|e_{mode}\rangle}\right)}. \quad (26)$$

Eigenvalue λ_- always has negative real part. The real part of eigenvalue λ_+ may have any sign. At relatively small n_0, we have $\mathrm{Re}\,\lambda_+ < 0$ whereas $\mathrm{Re}\,\lambda_+ > 0$ when parameter n_0 is above the threshold level. Therefore, threshold pump level n_0^{thr} can be calculated using formula $\mathrm{Re}\,\lambda_+ = 0$. Thus, we obtain

$$\langle e_{mode}|n_0^{thr}|e_{mode}\rangle = \frac{\hbar\langle e_{mode}|\mathrm{Im}\,\varepsilon|e_{mode}\rangle}{4\pi\tau_p|\vec{d}|^2}. \quad (27)$$

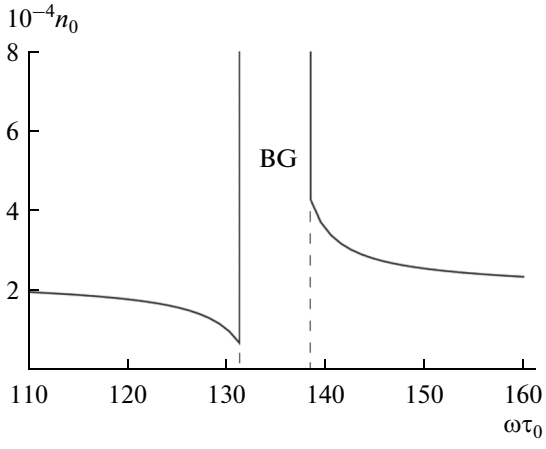

Fig. 2. Plot of threshold population inversion of lasing vs. frequency (BG is the band gap corresponding to a linear PC and $\tau_0 = \pi(d_1 + d_2)/c$).

It is seen that the lasing threshold depends on weighted imaginary part of permittivity $\langle e_{mode}|\mathrm{Im}\,\varepsilon|e_{mode}\rangle$ and population inversion $\langle e_{mode}|n_0|e_{mode}\rangle$ with the mode of the linear PC. Condition (27) shows that the lasing is started when the loss and gain averaged over the cavity mode are equal. Hence, the lasing threshold decreases when the field is concentrated in the layers with amplification. For the above PC parameters and the frequencies that are lower (higher) than the second band gap, the field in the crystal is concentrated in the gain (loss) layers, so that the threshold population inversions below and above the band gap are significantly different (Fig. 2). Such a dependence is a manifestation of the Borrmann effect in the PC [31, 32].

To find the field amplitude above the lasing threshold, we must take into account nonlinear effects in the

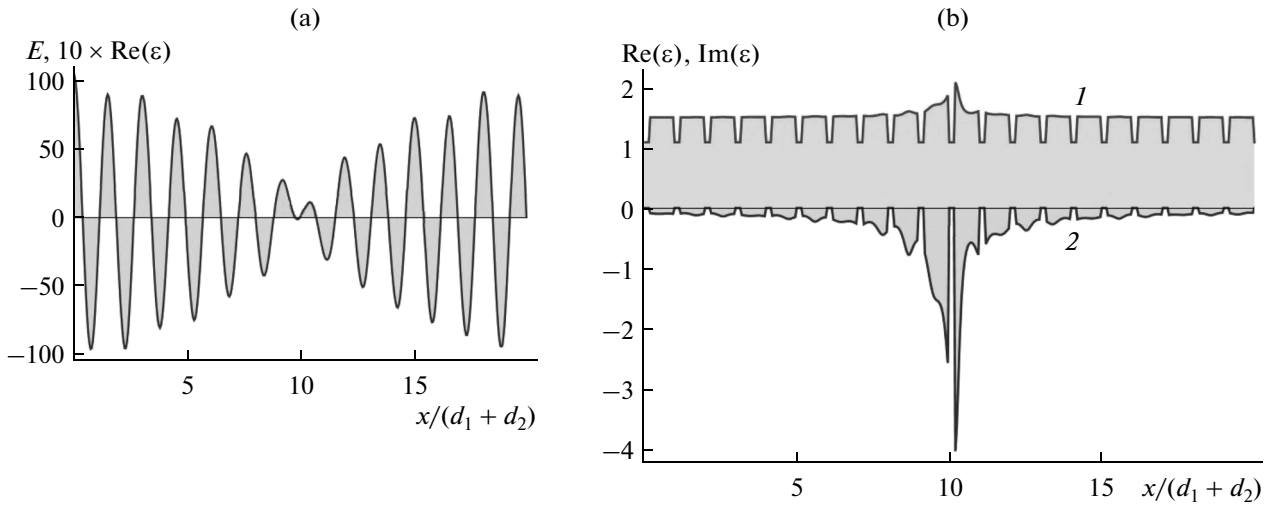

Fig. 3. (a) Electric field distribution in PC and (b) (*1*) real and (*2*) imaginary parts of the PC permittivity with allowance for nonlinearity of the gain medium (d_1 and d_2 are the thicknesses of layers in the PC cell, $\omega_{QD}\tau_0 = 90$ is the transition frequency in the gain medium, and $\tau_0 = \pi(d_1 + d_2)/c$).

system. The nonlinearity of the amplifying medium leads to a variation in the real part of permittivity, which may result in the field redistribution in the PC cell and violation of periodicity. However, the emission along the direction that is perpendicular to the surface is possible only if the dipole moments of metal nanoparticles exhibit in-phase oscillations, which is possible only in a periodic system.

We consider lasing in PC at frequencies from allowed band (Fig. 3a). The field distribution at the center of the allowed band is not spatially periodic in spite of the periodicity of the PC structure prior to lasing. This circumstance is due to the fact that the Bloch wavelength in the allowed band of PC is incommensurable with the PC period. Hence, the field causes nonuniform variations in the population inversion that lead to the secondary modulation of permittivity, which destroys the PC periodicity (Fig. 3b).

In the vicinity of the band gap, the wavelength of the laser mode is comparable with the PC period and the Bloch wave represents a modulated standing wave the period of which is close to the PC period. Figure 4a shows the electric field distribution upon lasing in the vicinity of the second band gap. Such a distribution exhibits a relatively high spatial periodicity, and the electric fields in the passive layers are matched. Hence, the emitters in such layers exhibit in-phase oscillations and the radiation is emitted along the direction that is perpendicular to the PC.

When the radiation loss is taken into account as the imaginary part of permittivity, we obtain dissipation in passive layers and structural modification of the band gap. However, the above properties of the field distribution (Fig. 4b) remain unchanged owing to the Borrmann effect [31]: the field is localized in the gain layers providing stability with respect to loss in the metal layers of PC. Normally, the field is not localized in the loss layers in the lasing regime. However, the system under study exhibits field localization in the loss layers.

The electric field generated in the PC induces dipole moments in nanoparticles. Assuming linear dependence of the induced dipole moments on the field inside nanoparticles, we calculate directional pattern of the radiation [33]

$$I(\vec{e}) = I^{(0)}(\vec{e})\left|\sum_n a_n \exp\left(-ik_0\vec{e}\cdot\vec{r}_n\right)\right|. \qquad (28)$$

For the emission along the direction that is perpendicular to the PC surface, the electric field in the loss layers must exhibit in-phase oscillations.[6] Such a scenario is possible if the phase shift per PC cell is a multiple of 2π. Therefore, the transition frequency of the gain medium must be tuned to the boundary of an even band gap of PC (Fig. 5).

2. FREQUENCY OF AMPLITUDE MODULATION IN VCSE AND DFB LASERS

The VCSE and DFB lasers are fabricated using the planar technology, so that the testing of lasers can be performed on the substrate at which they are produced and, hence, the production costs substantially decrease [12]. In addition, the surface from which the laser radiation is emitted may be plane-parallel in both lasers and the size of sample may be significantly less than the wavelength. Thus, a relatively narrow and symmetric directional pattern can be obtained.

[6] Recall that the loss layers simulate the perturbations causing scattering of electromagnetic waves that propagate along the surface.

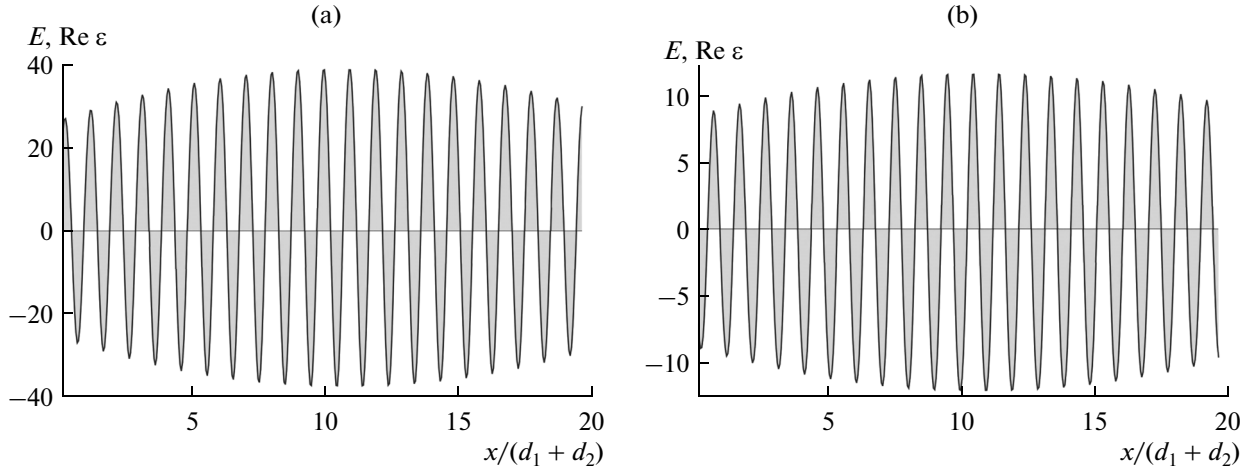

Fig. 4. Electric field distribution in PC for $\mathrm{Im}\,\varepsilon_2$ = (a) 0.0 and (b) 0.5 and transition frequency in gain medium $\omega_{QD}\tau_0 = 137$ ($\tau_0 = \pi(d_1 + d_2)/c$).

The DFB and VCSE lasers are used in optoelectronics for the transformation of electric signal. An important characteristic for such applications is the frequency of amplitude modulation in the presence of relatively small variations in the pump intensity that do not provide transition to the below-threshold regime [24, 34]. The frequency of the amplitude modulation is given by [24, 35] (see Appendix 2)

$$\omega_{am}^2 = \frac{g_0 S^{st}}{\tau_{en}} + \frac{\beta F_{mode}}{\tau_{en}\tau_{sp}}, \tag{29}$$

where $S^{st} = s/V_{mode}$ is the photon number density in the laser mode in the stationary state, s is the number of photons in a mode, V_{mode} is the mode volume, g_0 is the gain, $\tau_{en} = Q/\omega$ is the field-energy decay time in the cavity, τ_{sp} is the spontaneous decay time of the gain medium in free space, F_{mode} is the Purcell factor of the cavity mode, and β is the ratio of the rate of spontaneous decay to the cavity mode to the total rate of spontaneous decay. The mode volume is calculated as

$$V_{mode} = \frac{\int \varepsilon(\mathbf{r})|E(\mathbf{r})|^2\, dV}{\left(\varepsilon(\mathbf{r})|E(\mathbf{r})|^2\right)_{max}}, \tag{30}$$

where the integration is performed over the entire space and $\left(\varepsilon(\mathbf{r})|E(\mathbf{r})|^2\right)_{max}$ denotes the maximum value of the expression in parentheses in the entire space.

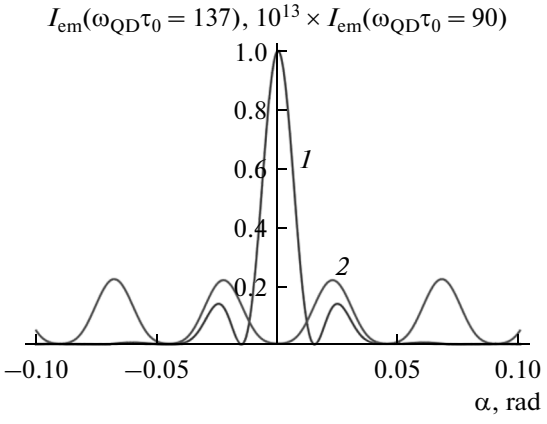

Fig. 5. Directional pattern of radiation for a periodic grating of NPs at $\omega_{QD}\tau_0$ = (*1*) 90 and (*2*) 137. The angle plotted on the abscissa axis is measured relative to the direction perpendicular to the PC plane, the number of PC cells is $N = 40$, the population inversion is $n_0 = 10^{-3}$, and the thicknesses of the layers in the PC cell are d_1 and d_2.

For both VCSE and DFB lasers, we have $\beta \ll 1$ owing to a relatively large number of modes to which QDs may emit. Therefore, we may approximate the modulation frequency as

$$\omega_{am} = \sqrt{g_0 \frac{s}{V_{mode}} \frac{\omega}{Q}}. \tag{31}$$

It is seen that the frequency of the amplitude modulation in the VCSE and DFB lasers is limited. Indeed, an increase in ω_{mode} results from an increase in number s of photons in the cavity mode that can be reached using an increase in either Q factor or population inversion. An increase in the Q factor leads to a decrease in the modulation frequency, so that such a method for an increase in the number of photons is inapplicable. An increase in population inversion n leads to an increase in the modulation frequency. However, the maximum possible population inversion is equal to the number density of atoms in the amplifying medium. In addition, the pump current that is needed for the generation of population inversion

$n = n_0$ exponentially increases with increasing n_0 [12]. Thus, the modulation frequency can hardly be increased using an increase in the population inversion. Note that a relatively high photon density in the cavity may cause overheating and the damage of gain medium.

An alternative approach to an increase in frequency ω_{am} employs a decrease in laser mode volume V_{mode}. In this case, the modulation frequency increases due to an increase in both photon density in the mode and spontaneous decay rate. Indeed, the rate of spontaneous decay of atom to the cavity mode differs from the decay rate in free space by Purcell factor [24]

$$F_{mode} = \frac{3}{4\pi^2}\frac{Q}{V_{mode}/(\lambda/n)^3}, \quad (32)$$

which is inversely proportional to the mode volume.

In conventional VCSE and DFB lasers, the mode volume is $V_{mode} \geq S\lambda/(2n)$, where S is the emitting surface and n is the refractive index for the cavity mode. Thus, the maximum frequency of the amplitude modulation is fundamentally limited in the VCSE and DFB lasers [12]. Wide-aperture sources of coherent radiation based on spasers are being developed at present to eliminate the above limitation.

3. SPASERS AND PLASMON DFB LASERS

3.1. Spasers

There has been considerable recent interest in the sources of coherent radiation based on composite materials containing plasmon nanostructures as alternatives to lasers with cavities based on PCs [5–11]. The key element of such structures is the generator of coherent plasmons (spaser) that was theoretically predicted in 2003 [10, 36] and experimentally implemented in 2009 [37, 38]. A spaser schematically represents a quantum–plasmon device consisting of inversely excited QDs, atoms, or molecules that interact with plasmon nanoparticles [10, 36], plasmon waveguides [37, 38], or surfaces. The working principle of spaser is similar to the working principle of laser based on the amplification provided by population inversion and the feedback provided by the stimulated emission of quantum system. The conditions for the stimulated emission of the inverse quantum system in the presence of the wave field that is generated in the same system are provided in the cavity that localizes the generated mode. Surface plasmons of nanoparticles the localization of which on a nanoparticle provides the conditions for positive feedback serve as the emitted field in the spaser. In other words, the generation of near-fields of nanoparticles takes place in a spaser. The amplification of surface plasmons results from the nonradiative energy transfer [39] from QDs. The process is based on the near-field interaction of a QD and a plasmon nanoparticle. Such a process can be considered as the basic process, since the probability of the nonradiative excitation of plasmon is greater than the probability of radiative emission of photon by factor $(kr_{NP-QD})^{-3}$, where $r_{NP-QD} \ll \lambda$ is the distance between the centers of nanoparticle and QD and $k = 2\pi/\lambda$. Ohmic loss I_J and the loss related to the far-field emission of electromagnetic fields I_{em} are the main losses in the spaser. The ohmic loss in nanoparticle increases proportionally to the nanoparticle volume ($I_J \sim V_{NP} \sim r_{NP}^3$), and the emission loss is proportional to the squared volume of nanoparticle ($I_{em} \sim V_{NP}^2 \sim r_{NP}^6$, r_{NP} is the radius of nanoparticle). Thus, the emission (ohmic) loss dominates at relatively large (small) sizes of nanoparticles when $r_{NP} \geq 50$ nm ($r_{NP} \leq 20$ nm).

The Purcell factor $F_{mode} \gg 1$ must be taken into account in spaser owing to a relatively small volume of the laser mode $V_{mode} \approx V_{NP} \ll \lambda^3$. If the frequency of the gain medium is tuned to the resonance with a mode of nanoparticle (e.g., dipole mode), the rate of spontaneous decay to such a mode is significantly higher than the total rate of the decay to the remaining modes ($\beta \approx 1$) (see Appendix 2). Therefore, frequency of the amplitude modulation ω_{am} in spaser may be significantly higher than the frequency in conventional lasers [40].

The main disadvantage of spasers that impedes their application as sources of far-field electromagnetic radiation is related to (i) low efficiency of the conversion of pump current energy into the radiation energy due to relatively high ohmic loss in nanoparticle and (ii) relatively wide directional pattern. The latter is due to the fact that the size of spaser is substantially less than the wavelength of emitted radiation, so that the directional pattern of a single spaser coincides with the directional pattern of a single dipole.

The sources of coherent radiation with a relatively narrow directional pattern can be based on the plasmon DFB lasers [19, 40] that employ the matching of planar distributed emitters (2D arrays of spasers [16, 17, 28, 30]) and the systems based on light stopping.

3.2. Plasmon DFB Lasers

Plasmon DFB lasers slightly differ from conventional DFB lasers. Therefore, they exhibit the main advantages and disadvantages of the conventional systems.

The lasing in plasmon DFB lasers takes place at waveguide modes that propagate along the surface of the system, and the radiation is emitted along the direction that is perpendicular to the generation plane. The positive feedback in the system results from multiple scattering by a periodic grating of perturbations (metal nanoparticles or holes in metal film).[7]

The plasmon DFB lasers are divided into two classes. The lasers of the first class are based on dielec-

[7] The grating of perturbations serves as the PC.

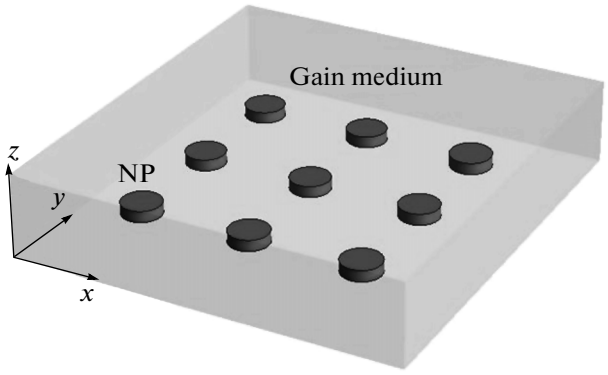

Fig. 6. Plasmon DFB laser in which the lasing takes place at the photonic modes that propagate along the dielectric film.

tric films with embedded periodic arrays of nanoparticles (Fig. 6). The photonic modes of dielectric film serve as the waveguide modes in such systems [9, 28]. The dielectric film contains the gain medium and a grating of metal nanoparticles that provides the positive feedback and the outcoupling of radiation from the plane of generation. Such systems differ from conventional DFB lasers by the application of a grating of metal perturbations instead of a grating of dielectric perturbations.

In the lasers of the second class, the cavity represents a metal film perforated with a grating of nanoholes [8, 41] (Fig. 7). In such systems, surface plasmons that propagate along the interface of metal film serve as laser modes and holes in the film serve as perturbations.

The narrowing of the directional pattern along the direction that is perpendicular to the plane of the plasmon DFB laser has been experimentally observed for both metal film perforated with periodic holes and covered with an amplifying layer [8, 41] and regular grating of metal nanoparticles in an amplifying layer [9, 28]. The presence of metal in the experimental samples leads to significant loss and relatively low Q factor of the system, so that the plasmon DFB lasers must be thresholdless lasers [42]. In other words, the lasing threshold in such lasers must be smoothed by the noise component. Nevertheless, the experiments yield a sharp threshold with respect to the radiation intensity induced by nanoparticles. Such a result is easy to interpret with allowance for the fact that the noise component of electromagnetic field in the system is a random component, so that the phase of the corresponding field is changed from particle to particle. Therefore, the radiation related to the noise component is emitted to the full solid angle. At the same time, electric and magnetic fields on all nanoparticles are matched upon lasing, so that a narrow directional pattern is obtained. Thus, the emission exhibits sharp threshold dependence on the pump intensity in spite of the fact that the plasmon DFB lasers are thresholdless lasers.

3.3. Spasing in the Stopped-Light Regime

Coherent sources with a narrow directional pattern based on the plasmon DFB lasers can be supplemented with the systems based on light stopping. In such structures, the lasing takes place at modes with zero group velocity.

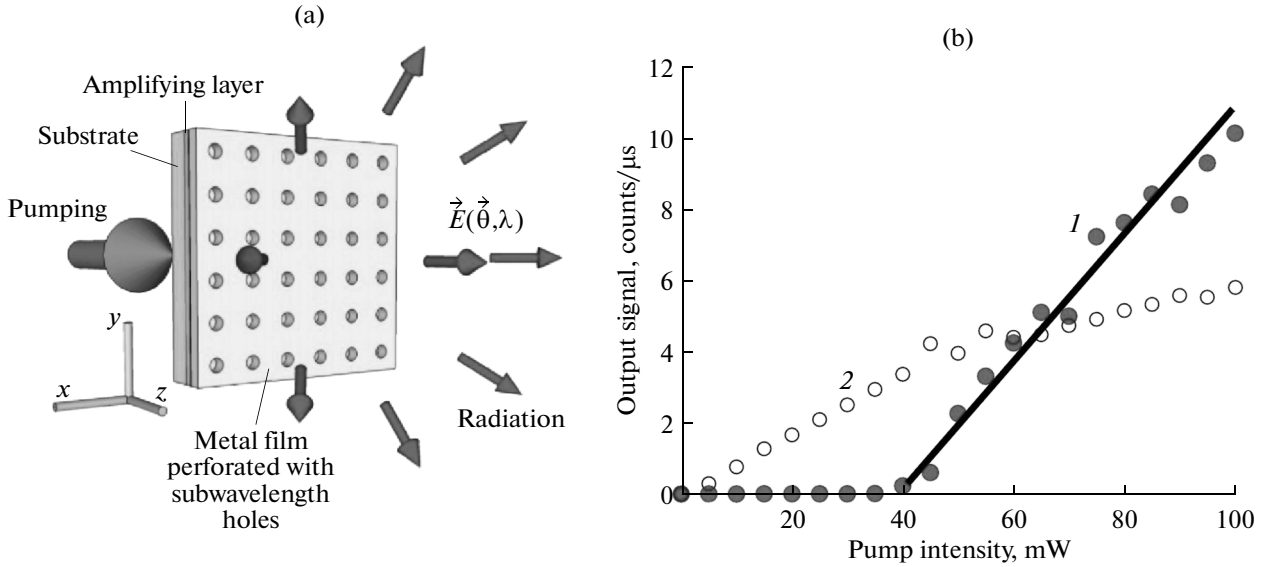

Fig. 7. (a) Plasmon laser in which the lasing takes place at plasmon modes of metal film (the distance between holes in metal film is one wavelength of radiation) and (b) plots of (solid circles) radiation intensity of the plasmon DFB laser and (open circles) luminescence intensity multiplied by a factor of 25 vs. pump intensity [8].

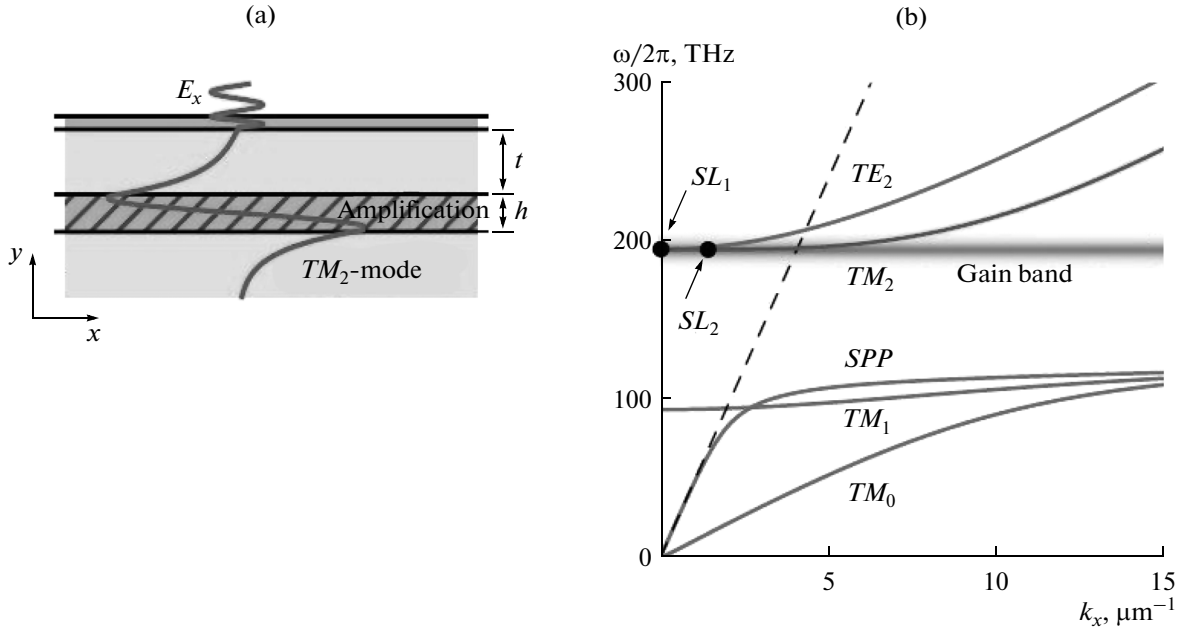

Fig. 8. (a) Layered planar structure that provides stopped light and (b) dispersion curves of plasmon modes for such a structure [43].

When group velocity in the system $v_{gr} = \partial\omega/\partial k$ approaches zero, density of states of electromagnetic field $\rho \sim \partial k/\partial\omega = 1/v_{gr}$ increases, so that the rate of induced transitions in the gain medium increases in the presence of such a light field. The stopped-light mode serves as the cavity mode and provides the feedback. The main principle of lasing based on stopped light lies in the fact that the group velocity of photon in the system is zero (i.e., the photon does not propagate being localized in a certain region in the system). Thus, the stimulated emission takes place also to the stopped photon. The stopped-light effect localizes the mode and allows lasing in a homogeneous infinitely long system in the absence of a real cavity that confines optical radiation. Such a type of lasing allows generation on the subwavelength scale.

A particular system is considered in [43] where the dynamics of lasing in a plasmon structure that has a slow-light mode in the near-IR range is analyzed. It is known that the slow-light regime can be reached in PCs and metamaterials [44]. The results of [43] show that a layered plasmon structure also makes it possible to generate stopped-light mode. In such a system stopped light emerges owing to the equalization of energy fluxes that are oppositely directed in the layers of the structure. Different directions of energy fluxes in the layers are needed for the generation of the surface plasmon. The group velocity becomes zero at the point of equalization of energy fluxes, since the energy density remains finite [45]. The fluxes cannot be mutually compensated in a passive or active system due to the presence of an energy flux that is related to dissipation or generation. However, an increase in gain in the passive medium may compensate for loss, so that the zero group velocity can be reached.

A metal–insulator–metal structure has been proposed in [43] for implementation of the stopped-light regime (Fig. 8a). The thickness of the upper metal layer was $t = 500$ nm, and the thickness of the dielectric layer was $h = 290$ nm. The insulator was placed on top of the thick metal layer. The TM_2 mode in the structure provides two points at which the group velocity is zero (Fig. 8b). A variation in the parameters of waveguide makes it possible to obtain such points at frequencies that are close to each other, so that a relatively large fragment with zero group velocity is formed on the dispersion curve $\omega(k)$ (Fig. 8). Both points are located on the dispersion curve in the region corresponding to leaky waves that are emitted to free space perpendicularly to the planar structure (Fig. 8a).

To compensate for the loss related to the emission along the direction perpendicular to the plane of structure and Joule loss in metal, a gain medium can be used instead of the insulator [46–48]. The dynamics of the pumped planar structure has been studied with the aid of numerical simulation of the Maxwell–Bloch equations [25]. The active medium has been simulated as a four-level system. In such an approach, we may assume that the pumping of active medium can be performed with the aid of a waveguide at a higher (optical) frequency.

The dispersion relations are obtained at different pump levels in the active medium. At an inversion of $n_{thr} = 0.13$, the imaginary part of the wave vector of the TM_2 mode changes sign. Such a level of the inversion is considered in [46–48] as the lasing threshold. The

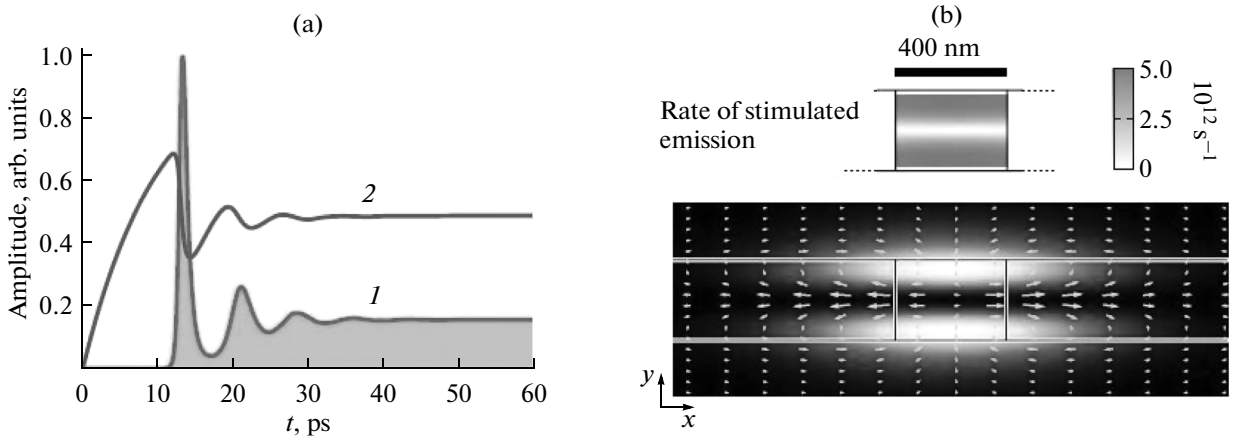

Fig. 9. (a) Plots of (*1*) field energy and (*2*) population inversion vs. time and (b) field distribution inside the waveguide upon lasing [43].

narrowing of the laser line has been demonstrated. In the steady-state regime, the inversion in the active medium $n \sim 0.5$ (Fig. 9a) is significantly greater that threshold level n_{thr} calculated above. Such an increase is due to the additional compensation for loss upon lasing (i.e., partial propagation of energy along the waveguide that results from both group-velocity dispersion and the formation of spatial wells caused by nonuniform distribution of electric field (Fig. 9b)).

Note that, in this case, the real part of the wave vector is close to zero, so that the atomic oscillations in the gain medium are matched in the spot the size of which is inversely proportional to the real part of the wave number. In fact, the size of the lasing spot is determined by the pumping area and has subwavelength size, which impedes the formation of a narrow directional pattern.

Note also a possibility of spasing in the stopped-light regime for the plasmon mode that is located on the dispersion curve outside the light cone and does not emit to free space. For example, the point with zero group velocity is observed for the TM_1 mode in the waveguide with a similar (metal–insulator–metal) structure and specific parameters of layers. In this case, the waves with $k \approx k_2$ (k_2 is the wave number of the TM_1 mode with zero group velocity) are involved in the formation of the laser mode. Therefore, the electromagnetic field of such a mode is modulated at a frequency of about $\sim\pi/k_2$. In this case, the emission is absent and the near-field is generated. Thus, such a regime can be called spasing in the absence of cavity.

3.4. Phase-Matching of a 2D Array of Spasers

2D spaser arrays can also be used for the development of coherent sources with relatively narrow directional patterns. In accordance with the recent theoretical predictions of [5, 6, 49–51], the interaction of spasers in a planar array may lead to phase matching of the field oscillations on single spasers and the narrowing of the directional pattern along the direction perpendicular to the plane of array.

In fact, such systems represent PCs a unit cell of which contains a scatterer surrounded by active medium. The plasmon resonance emerges in the scatterer at a certain frequency, a single cell is transformed into a spaser, and the system becomes similar to the system of [49–51]. The difference lies in the fact that the analysis cannot be restricted to the dipole–dipole interaction of the spasers.

Two substantially different methods can be used for mode locking in the 2D spaser array.

A rectangular grating of plasmon nanoparticles with complicated shapes (Fig. 10) that are placed on the surface of the active medium has been considered in [5, 6]. For certainty, we assume that the grating belongs to the *xy* plane and the edges of grating are parallel to the *x* and *y* axes.

Owing to the periodicity of the grating, the field in such a system can be represented as a series in terms of standing waves with wave numbers

$$\{k_x, k_y\} = \left\{\frac{\pi d_x}{L_x} n_x, \frac{\pi d_y}{L_y} n_y\right\},$$

where d_x and d_y are the distances between the neighboring nanoparticles along the *x* and *y* axes, respectively; L_x and L_y are the sizes of the system along the axes; and n_x and n_y are the integers that range from 0 to L_x/d_x and from 0 to L_y/d_y, respectively.

The shape of nanoparticles in [5, 6] corresponds to the minimum radiation intensity of the grating of nanoparticles when the field distribution in the system coincides with the standing wave with $\{k_x, k_y\} = \{0,0\}$ (phase matching). For such a shape of nanoparticles, the threshold pumping for the phase-matched mode is

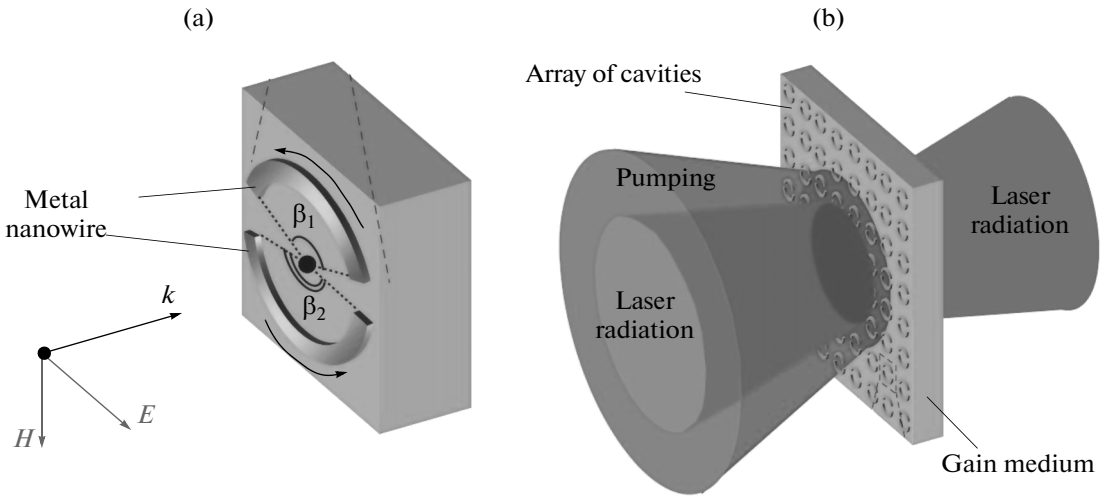

Fig. 10. Schemes of (a) NP and (b) NP array [5].

lower than the pumping for any mode of the system. In any system of several spasers, which represents a multimode laser, the mode competition results in the survival of the mode with the lowest pumping threshold and the phase-matched distribution of currents is established in the system. Note two significant disadvantages of such a method (the application of nanoparticles with complicated shapes (Fig. 10a) and the minimization of the radiation intensity for the above type of phase matching) that impede the development of an efficient source of coherent radiation.

A method for the phase-matching of the oscillations of dipole moments of single nanoparticles in a 2D spaser array that is free of the above disadvantages has been proposed in [49–51]. In such a method, at least two nanoparticles interact with each QD in the spaser array [49–51]. Such interaction in the system of spasers leads to the phase matching of the oscillations of spasers that is maintained when the radiative loss is taken into account. The radiation power of an array of phase-matched spasers per unit solid angle along the direction perpendicular to the plane of array is proportional to the square of the number of spasers N^2. Such an increase is due to superradiance [52] at small sizes of the system (significantly less than the wavelength) and the narrowing of the directional pattern at large sizes. Thus, the system may serve as an efficient source of directional coherent radiation.

We consider a particular 2D periodic array of spasers. Two inverse QDs that are located in the vicinity of a metal ellipsoid nanoparticle (NP) (Fig. 11a) serve as a model of spaser [49–51]. For simplicity, we assume that the quantum system is a two-level system and the ellipsoid nanoparticles that have dipole plasmon modes serve as cavities. The eigenfrequencies of the dipole modes with different orientations are different owing to the nonspherical shape of the nanoparticles. We assume that the frequency of the mode with the dipole mode that is oriented along the major axis of ellipsoid coincides with the QD transition frequency and the frequencies of the remaining dipole modes substantially differ from the transition frequency and, hence, are not excited upon lasing in the system.

Let single spasers [49–51] form a 2D rectangular grating. For definiteness, we assume that the grating belongs to the xy plane and the edges of the grating are parallel to the x and y axes (Fig. 11c). We also assume that the distances between the nanoparticles along the x and y axes (δx and δy in Fig. 11b) are significantly less than the wavelength ($\Delta = \delta x = \delta y = \lambda/20$ in [49–51]) and the system under study has a square shape with side L and number of spasers N.[8]

The spaser dynamics is described using a system of three equations for amplitude of NP dipole moment a, polarization σ, and population inversion D of QD [53]. In the 2D array, the spaser with number $\vec{n} = (n_x, n_y)$ interacts with the local field $\Omega_{\vec{n}-\vec{m}} \cdot a_{\vec{m}} = \Omega((\vec{n}-\vec{m})\Delta) \cdot a_{\vec{m}}$ that is generated by the spaser with number $\vec{m} = (m_x, m_y)$. The projection of the local field of a single dipole along the direction of the dipole moment of the nanoparticle is represented as

$$\Omega(\vec{e}R) = \tau_{\text{rad}}^{-1}\left(\frac{3(\vec{e}\cdot\vec{e}_x)^2 - 1}{R^3} - ik_0\frac{3(\vec{e}\cdot\vec{e}_x)^2 - 1}{R^2} - k_0^2\frac{(\vec{e}\cdot\vec{e}_x)^2 - 1}{R}\right)\exp(ikR), \quad (33)$$

where $k_0 = \omega/c$ is the wave number in vacuum, $\vec{e}_x$ is the unit vector that is parallel to the NP dipole moment, $\vec{e}R$ is the vector that connects spaser with number $\vec{m}$

[8] A p–n junction can be used in practice as amplifying medium instead of QDs. In this case, the p–n junction is formed on a specific substrate (e.g., InP) and, then, metal (gold or silver) NPs are deposited on the p–n junction.

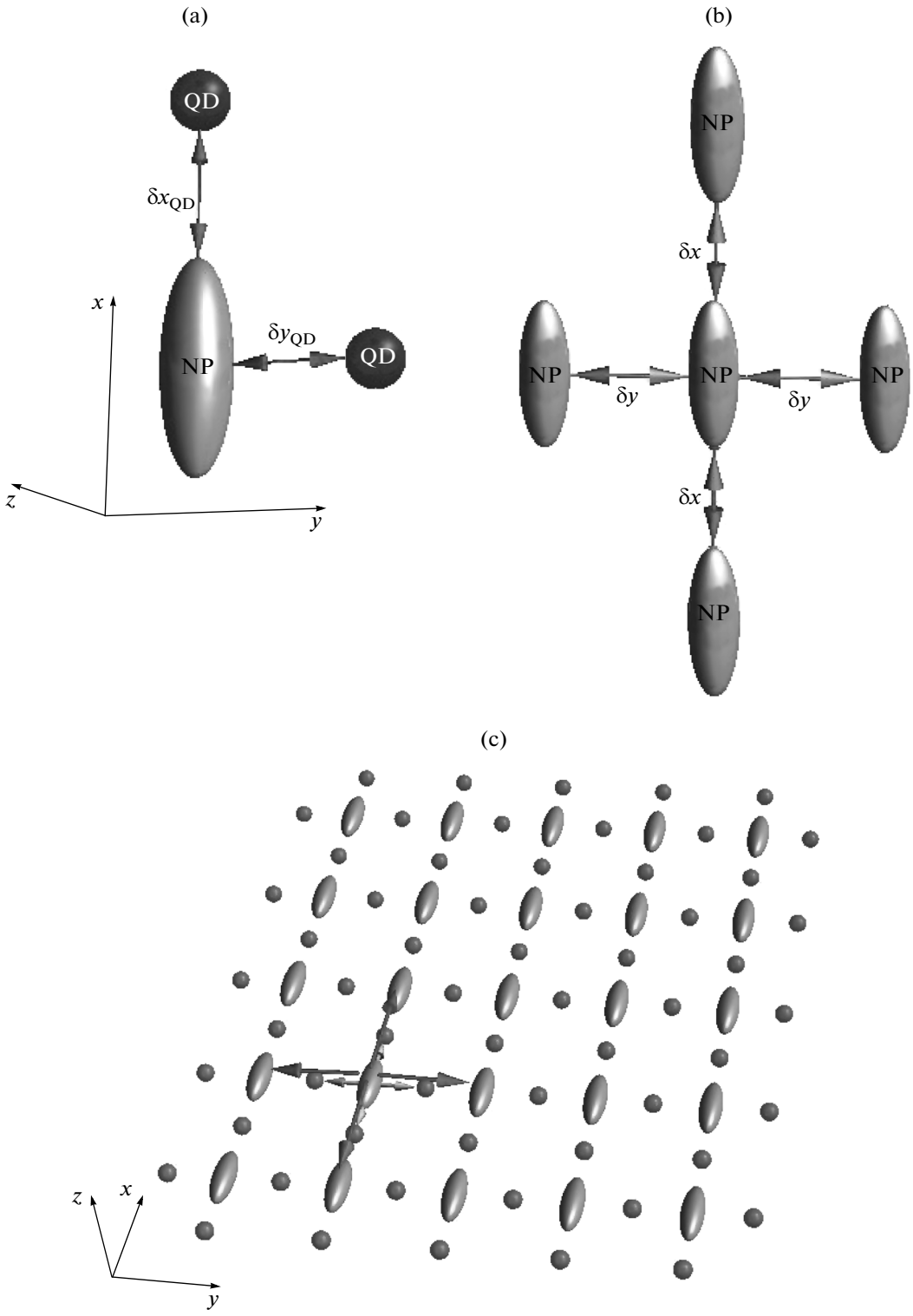

Fig. 11. (a) Scheme of a unit cell of a spaser array: ellipsoid NP that interacts with two QDs. (b) Mutual positions of neighboring NPs in the spaser array. (c) Phased array of spasers (the arrows show NPs (ellipsoids) and QDs (spheres) that interact with the central NP).

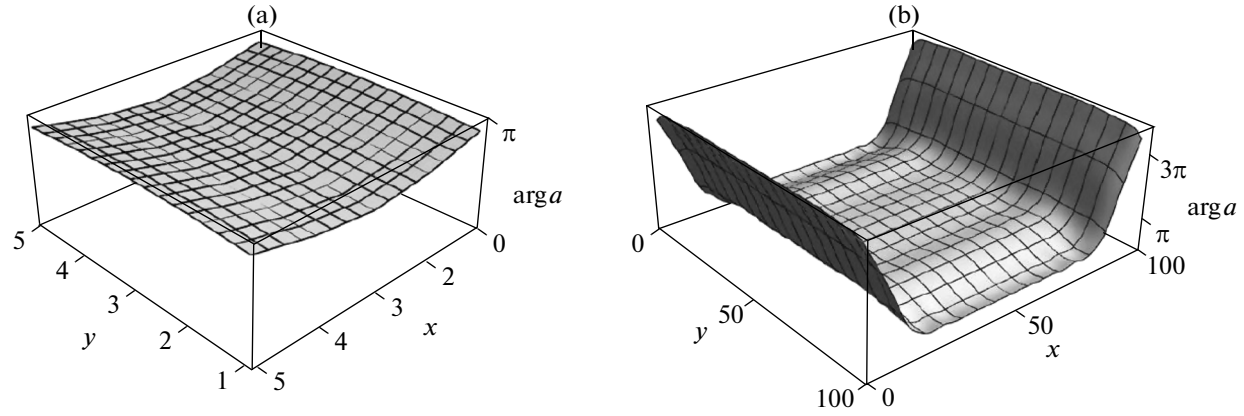

Fig. 12. Distributions of the oscillation phases of dipole moments over the spaser array for (a) 5×5 and (b) 100×100 spaser arrays at $\Omega_r \neq 0$ (spaser numbers are plotted on the x and y axes, and the phase of the dipole moment is plotted on the z axis).

and spaser with number $\vec{n}$, and τ_{rad}^{-1} is the radiative decay rate. For a spherical nanoparticle with radius r_{NP} in free space, we have $\tau_{rad}^{-1} = 2\dfrac{(k_0 r_{NP})^3}{\partial\varepsilon/\partial\omega}\Big|_{\omega=\omega_{res}}$ [53]. In general, parameter τ_{rad}^{-1} depends on the environment and shape of NP. At the frequency of the dipole resonance ω_{res}, parameter τ_{rad}^{-1} is related to polarizability $\alpha(\omega)$:

$$\tau_{rad}^{-1} = -\frac{2}{3}\frac{k_0^3}{\partial\alpha^{-1}/\partial\omega}\Big|_{\omega=\omega_{res}}.$$

For the calculation of the local field, we restrict consideration to the dipole–dipole interaction (with allowance for the retardation effect (33)) of the nanoparticles and disregard the interaction with higher multipoles. The expression for the local field is typical of free space, and a single effect that is related to the metal film and taken into account is the wave decay in free space (we have $k = k' + ik''$ in expression (33), and $k' = k_0$ and $k''/k' = 0.2$ in the numerical simulation). When such a decay is not taken into account, the NP interaction in a perfect system is not reduced to the interaction of neighboring NPs, the finiteness of the sizes of structure becomes significant, and we obtain nonuniformity over the array of local fields that are exerted on spasers and several instabilities. As for the remaining effects, the qualitative influence of the local field on the system under study is absent.

In the approximation of rotating wave [54–58], the system of interacting spasers is described using the system of nonlinear differential equations

$$\dot{a}_{\vec{n}} + \tau_{dnp}^{-1} a_{\vec{n}} = -i\Omega_r \sum_{|\vec{n}-\vec{m}|=1} \sigma_{\vec{m}} + i\sum_{\vec{m}\neq\vec{n}} \Omega_{\vec{n}-\vec{m}} a_{\vec{m}}, \qquad (34)$$

$$\dot{\sigma}_{\vec{n}} + \tau_{dqd}^{-1}\sigma_{\vec{n}} = i\Omega_r \sum_{|\vec{n}-\vec{m}|=1} a_{\vec{m}} D_{\vec{m}}, \qquad (35)$$

$$\dot{D}_{\vec{n}} + \tau_{iqd}^{-1}(D_{\vec{n}} - D_0) = 2i\Omega_{rl} \sum_{|\vec{n}-\vec{m}|=1} (a_{\vec{m}}^*\sigma_{\vec{n}} - a_{\vec{m}}\sigma_{\vec{n}}^*), \qquad (36)$$

where $a_{\vec{n}}$ is the dipole moment of the $\vec{n}$th nanoparticle, $\sigma_{\vec{n}}$ is the dipole moment and $D_{\vec{n}}$ is the population inversion of the $\vec{n}$th QD, and D_0 is the external pump intensity that is assumed to be equal for all QDs. The relaxation times of polarization (transverse relaxation) and population inversion (longitudinal relaxation) of QDs are τ_{dqd} and τ_{iqd}, respectively. The lifetime of the plasmon mode is determined by the Joule and radiative losses: $\tau_{dnp}^{-1} = \tau_J^{-1} + \tau_{rad}^{-1}$ (in the calculations, we use $\tau_J^{-1} = 27\tau_{rad}^{-1}$).

In the system of equations (34)–(36), we take into account the interaction of NPs (the second term on the right-hand side in Eq. (34)) and the interaction of NP with four neighboring QDs (the first term on the right-hand side in Eq. (34)). We also take into account the radiative loss that increases with an increase in the number of spasers. The system of equations (34)–(36) does not take into account the spontaneous emission of QDs that is important in the vicinity of the generation threshold. Hence the above system of equations can be used only substantially above the lasing threshold.

The numerical solution of the system of equations (34)–(36) at Ω_R that is significantly greater than a certain threshold level shows that the oscillations of dipole moments of single spasers in the spaser array reach a stationary level with almost uniform phase distribution over the array (Fig. 12). In the arrays with a number of spasers N of about 10^2, we can reach almost perfect phase matching of the oscillations of dipole moments in the system (Fig. 12a). In relatively large systems ($N \gg 10^2$), we obtain perturbations in the vicinity of boundaries along the direction that is parallel to the oscillations of dipole moments (Fig. 12b). Such an edge effect has a scale of about one wavelength in vacuum. When the sizes of the system are sig-

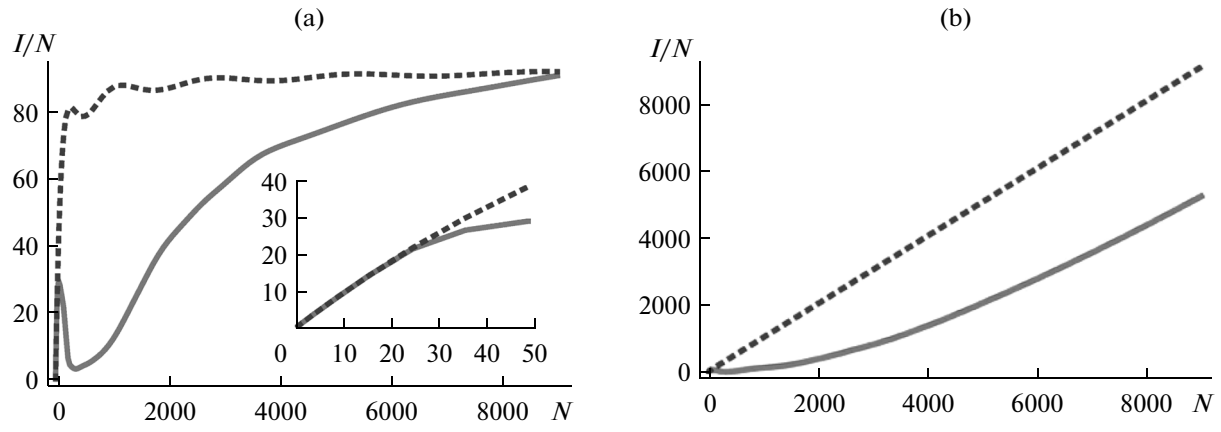

Fig. 13. Plots of (a) integral (with respect to angle) radiation intensity and (b) radiation intensity per one spaser along the direction that is perpendicular to the plane of array vs. number of spasers: (dashed lines) perfectly matched system and (solid line) real system. The inset shows the dependence for a relatively small number of spasers.

nificantly greater than the wavelength, the influence of the edge effects on the radiation intensity of a spaser array and the directional pattern is negligible.

The phase-matched regime of oscillations of the dipole moments in the spaser array is reached owing to the interaction of NPs and QDs of the neighboring NPs.

In the phase-matched regime, the far-field interaction of spasers leads to an increase in the radiation intensity. Such an effect is more developed for the systems with small sizes ($k_0R \ll 1$) for which expression (33) is represented as

$$\Omega(\vec{e}R) \approx \tau_{\text{rad}}^{-1}\left(\frac{3}{2}\frac{3(\vec{e}\cdot\vec{e}_x)^2-1}{R^3}+i\right), \tag{37}$$

where $\operatorname{Im}\Omega(\vec{e}R) \approx \tau_{\text{rad}}^{-1}$. When the dipoles oscillate with identical phases and amplitudes, the last term in expression (34) can be divided into two parts:

$$\begin{aligned} i\sum_{\vec{m}\neq\vec{n}}\Omega_{\vec{n}-\vec{m}}a_{\vec{m}} &= ia_{\vec{m}}\sum_{\vec{m}\neq\vec{n}}\operatorname{Re}\Omega_{\vec{n}-\vec{m}} - a_{\vec{m}}\sum_{\vec{m}\neq\vec{n}}\operatorname{Im}\Omega_{\vec{n}-\vec{m}} \\ &= ia_{\vec{m}}\sum_{\vec{m}\neq\vec{n}}\operatorname{Re}\Omega_{\vec{n}-\vec{m}} - a_{\vec{m}}(N-1)\tau_R^{-1}. \end{aligned} \tag{38}$$

The second term on the right-hand side in expression (38) leads to an increase in the loss rate for the $\vec{n}$th plasmon by a factor of $(N-1)$. Hence, the effective decay rate is $\tau_{\text{J}}^{-1} + N\tau_{\text{rad}}^{-1}$ and Eq. (34) can be represented as

$$\begin{aligned} &\dot{a}_{\vec{n}} + \left(\tau_{\text{J}}^{-1} + N\tau_{\text{rad}}^{-1}\right)a_{\vec{n}} \\ &= -i\Omega_{\text{rl}}\sum_{|\vec{n}-\vec{m}|=1}\sigma_{\vec{m}} + i\operatorname{Re}\sum_{\vec{m}\neq\vec{n}}\Omega_{\vec{n}-\vec{m}}a_{\vec{m}}. \end{aligned} \tag{39}$$

Thus, the dipole moments of NPs at $k_0R \ll 1$ provide identical contributions to the radiation intensity of each NP: $\tau_{\text{rad\_eff}}^{-1} = N\tau_{\text{rad}}^{-1}$. In this case, the total radiation intensity of N NPs is proportional to the square of the total number N^2, which is typical of the superradiance [52]. Note that such a dependence is obtained with the aid of the expression for the total field of dipole with allowance for retardation (33). Therefore, all terms must be taken into account in expression (33) to correctly describe the effect of radiation on the oscillation dynamics of dipole moments in the spaser array.

The radiation power of the spaser array can be obtained using the equations of energy balance that follow from expression (39) for the stationary regime:

$$\begin{aligned} &\sum_{\vec{n}}\left[\Omega_{\text{r}}\operatorname{Im}(a_{\vec{n}}^*\sigma_{\vec{n}}) + \Omega_{\text{rl}}\sum_{|\vec{m}-\vec{n}|=1}\operatorname{Im}(a_{\vec{n}}^*\sigma_{\vec{m}})\right] \\ &= \tau_{\text{J}}^{-1}\sum_{\vec{n}}|a_{\vec{n}}|^2 + \sum_{\vec{n},\vec{m}}\operatorname{Im}(\Omega_{\vec{n}-\vec{m}})\operatorname{Re}(a_{\vec{n}}^*a_{\vec{m}}). \end{aligned} \tag{40}$$

In accordance with expression (37), we have $\operatorname{Im}\Omega(\vec{e}R) \approx \tau_{\text{rad}}^{-1}$ for $k_0R \ll 1$. Thus, the term $\vec{n} = \vec{m}$ in sum $\sum_{\vec{n},\vec{m}}$ can be taken into account as $\operatorname{Im}\Omega_{\vec{n}-\vec{m}} = \tau_{\text{rad}}^{-1}$. The left-hand side of Eq. (40) is proportional to the energy loss in the system. The first term on the right-hand side corresponds to the Joule loss, and the second term corresponds to radiative loss I:

$$I = \frac{m\omega^2}{q^2}\sum_{\vec{n},\vec{m}}\operatorname{Im}(\Omega_{\vec{n}-\vec{m}})\operatorname{Re}(a_{\vec{n}}^*a_{\vec{m}}), \tag{41}$$

where q is the electron charge. Figure 13a presents the dependence of the power of radiative loss on the number of spasers in the array.

At relatively small sizes of the system, the spasers exhibit the in-phase oscillations ($N < 10^2$ for the above parameters) (Fig. 12a). In this case, the radiation intensity per one spaser linearly increases with an increase in the number of spasers: $I_1 = I/N \sim N$. For

such arrays, the radiation intensity coincides with the radiation intensity of a perfectly phase-matched system (see inset to Fig. 13a). With a further increase in the size of the array, the radiation intensity decreases due to the formation of boundary states (Fig. 12b). A further increase leads to the phase-matching of the major part of the array (Fig. 12b). For the number of spasers $N > 5\times10^3$, the radiation intensity of the system under study becomes approximately equal to the radiation intensity of a perfectly matched system and the total radiation intensity decreases. Such a decrease results from the destructive interference of the dipole moments of spasers that are located in different parts of the system. The equality of the radiation intensities of the system under study and the perfectly matched system is due to negligible influence of the edge effects at relatively large sizes of the spaser array.

For practical applications, the total radiation intensity of the system of spasers is less important than the radiation intensity per unit solid angle along the direction perpendicular to the plane of array (i.e., the radiation power that is measured using a small detector that is placed above the plane of spaser array). We can calculate the total radiation power of the system of dipoles taking into account the interaction in the system via the total radiation field. However, such an approach is inapplicable in the calculation of the angular distribution of the radiation intensity. Such a distribution can be obtained with the aid of the electrodynamic analysis of radiation for the calculated distribution of amplitudes and phases of NP dipole moments in the phase-matched spaser array. In other, words, we consider a system of spasers as a phased antenna array. The angular distribution of the radiation of such an antenna can be obtained using the Fourier transform of the current distribution over its aperture [33]. For the system under study, we must use the distribution of phases and amplitudes of dipole moments over the system of spasers. Thus, the angular distribution of the radiation intensity is given by

$$I(\vec{e}) = I^0(\vec{e})\left|\sum_{\vec{n}} a_{\vec{n}} \exp\left(-ik_0\vec{e}\cdot\vec{r}_{\vec{n}}\right)\right|^2, \qquad (42)$$

where $\vec{e}$ is the unit vector along the direction of emission, $\vec{r}_{\vec{n}}$ is the coordinate vector of the $\vec{n}$ th dipole in the array, and $I^0(\vec{e}) = (8\pi)^{-1} ck_0^4 \left\|\vec{e}\times\vec{e}_x\right\|^2$ is the radiation intensity of a single dipole along vector $\vec{e}$. The integration of expression (42) over all directions **e** yields expression (41). Along the direction that is perpendicular to the plane, we have $I(\vec{e}) = I^0(\vec{e})\left|\sum_{\vec{n}} a_{\vec{n}}\right|^2$ and obtain dependence $I/N \sim N$ for the phase-matched system with any size.

Such a conclusion is proven by the results of numerical calculation (Fig. 13b). It is of interest that a linear increase in ratio I/N is determined by two effects. At relatively small sizes of the system ($L < \lambda$), such an increase results from an increase in the integral radiation intensity due to the superradiance [52]. At $L > \lambda$, an increase in ratio I/N is caused by the narrowing of the directional pattern due to an increase in the aperture of the emitting system (Fig. 14).

The numerical study of the 2D spaser array shows that the interactions of NPs with QDs of the neighboring NPs leads to the phase-matching of the oscillations of dipole moments of single spasers. A mode with the lowest threshold with respect to pumping D_{thr} normally survives in multimode lasers in the presence of mode competition [49, 50, 54–59]. For the system of spasers, the threshold with respect to pumping is given by

$$D_{\text{thr}}(\vec{k}) = \Omega_{\text{r\_eff}}^{-2}\tau_{\text{dnp\_eff}}^{-1}\tau_{\text{dqd}}^{-1}\left(1+\delta_{\text{eff}}^2\tau_{\text{dnp\_eff}}^2\right).$$

Such a threshold is identical to the threshold of a single spaser [53] with effective parameters Ω_{r}, τ_{dnp}, and mismatch δ

$$\Omega_{\text{r\_eff}} = 2\Omega_{\text{r}}\left(\cos k_x\Delta + \cos k_y\Delta\right), \qquad (43)$$

$$\tau_{\text{dnp\_eff}}^{-1} = \tau_{\text{J}}^{-1} + \Delta^{-2}\int\Omega(\vec{e}R)\,d^2\vec{R}, \qquad (44)$$

$$\delta_{\text{eff}} \approx 3\tau_{\text{rad}}^{-1}\left(k_0\Delta\right)^{-3}\left(2\cos k_x\Delta - \cos k_y\Delta\right), \qquad (45)$$

where $\vec{k} = (k_x, k_y)$ is the wave number of the eigenmode of dipole oscillations in the spaser array.

Quantity $D_{\text{thr}}(\vec{k})$ depends on three factors $\Omega_{\text{r\_eff}}^{-2}$, $\tau_{\text{dnp\_eff}}^{-1}$, and $\left(1+\delta_{\text{eff}}^2\tau_{\text{dnp\_eff}}^2\right)$. The first term $\Omega_{\text{r\_eff}}^{-2}$ exhibits minimum at $|\vec{k}| = 0$. Indeed, in the phase-matched mode, the fields of the neighboring NPs interfere on QDs, so that the corresponding interactions and energy transfer reach maximum levels for the phase-matched mode. Such an effect has been analyzed in [50]. On the other hand, the second term $\tau_{\text{dnp\_eff}}^{-1}$ increases with increasing $|\vec{k}|$ owing to an increase in the radiative loss, so that quantity D_{thr} increases. With regard to this factor, the mismatched mode must have the lowest threshold. At the same time, the third term $\left(1+\delta_{\text{eff}}^2\tau_{\text{dnp\_eff}}^2\right)$ tends to unity when parameter $\tau_{\text{dnp\_eff}}^{-1}$ increases.

Thus, the stationary mode in the system results from the competition of two effects: phase-matching related to the nonlinear dipole–dipole interaction of NPs with neighboring QDs and mismatching related to an increase in the radiation intensity.

The first effects dominates at realistic parameters. Hence, the mode with $|\vec{k}| = 0$ has the lowest threshold and will be observed in the stationary regime.

The above theory can be used only for an infinite 2D array of spasers, since, in accordance with the assumption, the threshold and frequency of lasing are identical for all of spasers in the array. A system with

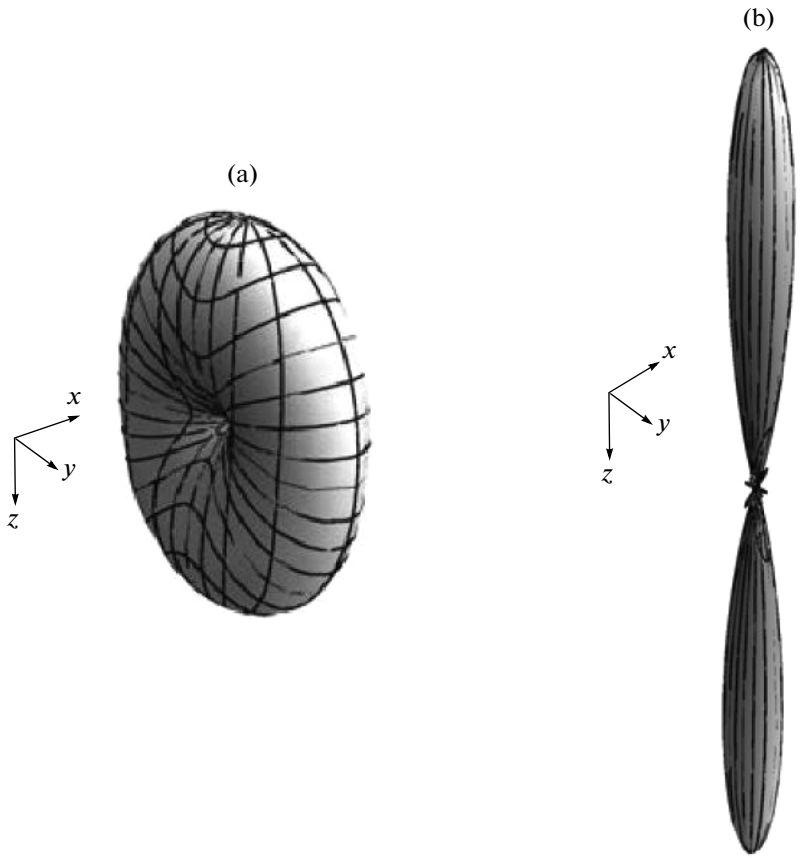

Fig. 14. Directional pattern for the phase-matched spaser array for the system of (a) 5 × 5 and (b) 100 × 100 spasers.

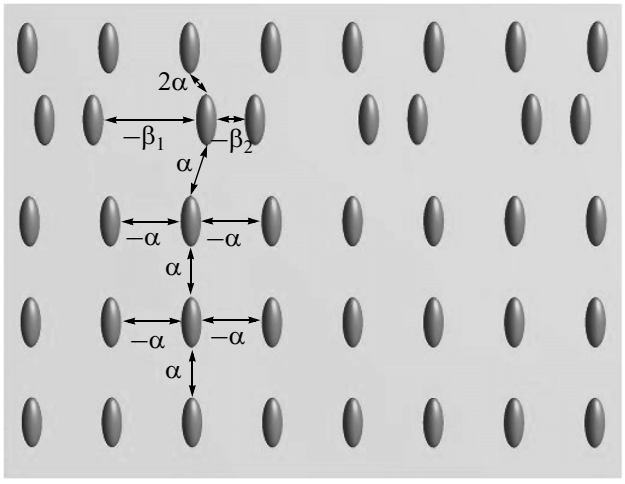

Fig. 15. Position of NPs in the vicinity of the boundary of the phase-matched spaser array at which the field on NPs does not depend on the NP position in the array at $\alpha = |\vec{d}|/\delta y^3$, $\beta_1 = |\vec{d}|/(1.2636\delta y)^3$, and $\beta_2 = |\vec{d}|/(0.7364\delta y)^3$, where $\delta x = \sqrt[3]{2}\delta y$ and δy are the distances between the neighboring NPs along the directions that are perpendicular and parallel to the boundary of array, respectively.

finite sizes exhibits edge effects at the boundaries (Fig. 12b) that lead to a decrease in the radiation intensity when the size of structure is on the order of wavelength (Fig. 13a).

The edge effects are due to the shift of the frequency of the plasmon resonance of NPs at the boundaries relative to the resonance frequency of NPs at the center of the array. Indeed, the frequency of the NP plasmon resonance depends on the environment. At the center of the system, the environments are identical and, hence, the shifts of the resonance frequency are also identical. For the spasers at the boundaries, the environment differs from that at the center of the system, so that the frequency of the NP plasmon resonance at the boundary differs from the resonance frequency of the same NP that is located at the center.

To compensate for the edge effects in the array, we must change the mutual positions of NPs at the edges of the system in such a way that the frequencies of plasmon resonances become identical. Figure 15 shows the positions of NPs at the boundary of the array at which the resonance frequencies are identical for all NPs.

In the resulting system, the presence of boundary does not affect the phase distribution of dipole

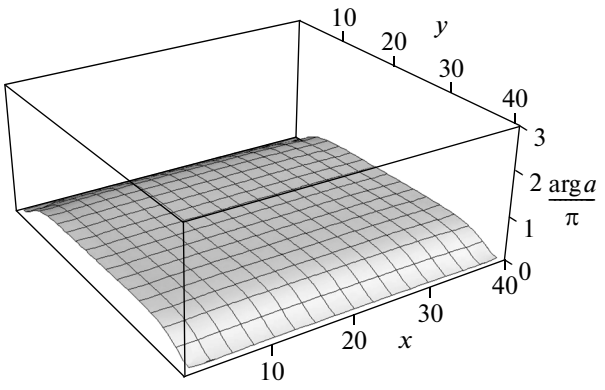

Fig. 16. Distribution of the oscillation phases of dipole moments over the spaser plane for the 40×40 spaser array in which the edge effects along the x axis are compensated for (see Fig. 15).

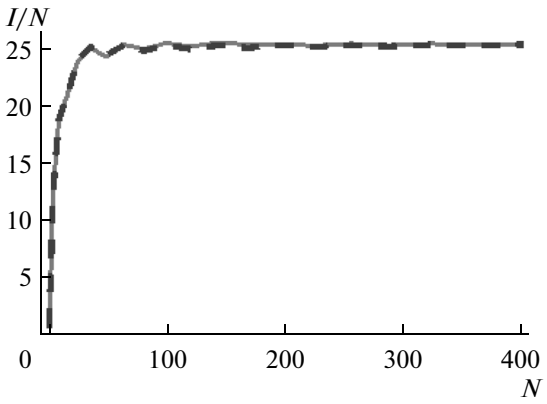

Fig. 17. Plots of radiation intensity per one spaser in the phase-matched array vs. number of spasers for (dashed line) perfectly matched and (solid line) real systems.

moments. The results of numerical simulation prove such a conclusion (Fig. 16).

Thus, the radiation intensity of the system under study and a perfectly matched system coincide at any number of spasers in the array (Fig. 17).

CONCLUSIONS

Modern plasmon wide-aperture lasers [9, 28, 41] predominantly represent plasmon DFB lasers. Such lasers exhibit the generation of the Bloch wave at the edge of the second band gap. Plasmon DFB lasers are free of strict limitations on the frequency of the amplitude modulation that are typical of DFB and VCSE lasers. Thus, the former, can be used in optoelectronics for transformation of electric signal into optical signals and vice versa.

Devices based on cooperative phase-matching of emitters with the generation of a wave with zero tangential wave vector may serve as alternatives to the plasmon DFB lasers. Note, for example, lasers with cavities on the stopped-light mode and 2D spaser arrays.

The main principle of lasing with the aid of stopped light is based on the fact that the group velocity of photons in such devices is zero, so that photons do not propagate and appear to be localized in certain region inside the system. The resulting stimulated emission takes place to the same stopped photons, so that the lasing can be obtained in homogeneous infinitely long medium in the absence of a real cavity that confines the radiation. Such an effect allows lasing on the subwavelength scale.

In a 2D spaser array, the interaction of NPs via QDs of the neighboring spasers may lead to the phase-matching of the oscillations of dipole moments of single NPs. When the aperture of the array is sufficient, the directional pattern becomes relatively narrow and the total radiation intensity increases by two orders of magnitude due to superradiance. Such devices are interesting for applications in systems of open optical communications. In particular, the first optical phased array can be developed.

APPENDIX 1

BAND STRUCTURE OF PC

PCs represent structures in which the permittivity exhibits periodic variation along one, two, or three axes in space. PCs are classified as 1D, 2D, and 3D with respect to the number of directions along which the permittivity is varied.

The properties of a linear 1D PC are well studied, the electric-field distribution in such a structure satisfies the Floquet–Bloch theorem: $E_y(x) = \exp(ik_B x) f(x)$, where $f(x) = f(x + L)$ and k_B is the Bloch wave number. When the PC consists of two alternating layers with thicknesses d_1 and d_2, permittivities ε_1 and ε_2, and permeabilities μ_1 and μ_2, respectively, the Bloch wave number can be calculated using the Rytov formula [30]

$$\cos(k_B(d_1 + d_2)) = \cos(k_1 d_1)\cos(k_2 d_2) - \frac{1}{2}\left(\frac{Z_1}{Z_2} + \frac{Z_2}{Z_1}\right)\sin(k_1 d_1)\sin(k_2 d_2), \quad \text{(A1.1)}$$

where $k_1 = \omega\sqrt{\varepsilon_1\mu_1}/c$ and $k_2 = \omega\sqrt{\varepsilon_2\mu_2}/c$ are the wave vectors in the first and second media, respectively, and Z_1 and Z_2 are the corresponding impedances. The presence of band gaps (BGs) in the spectrum is an important property of PCs. Electromagnetic waves with frequencies from BG exponentially decay in the depth of PC, the real part of the Bloch wave number

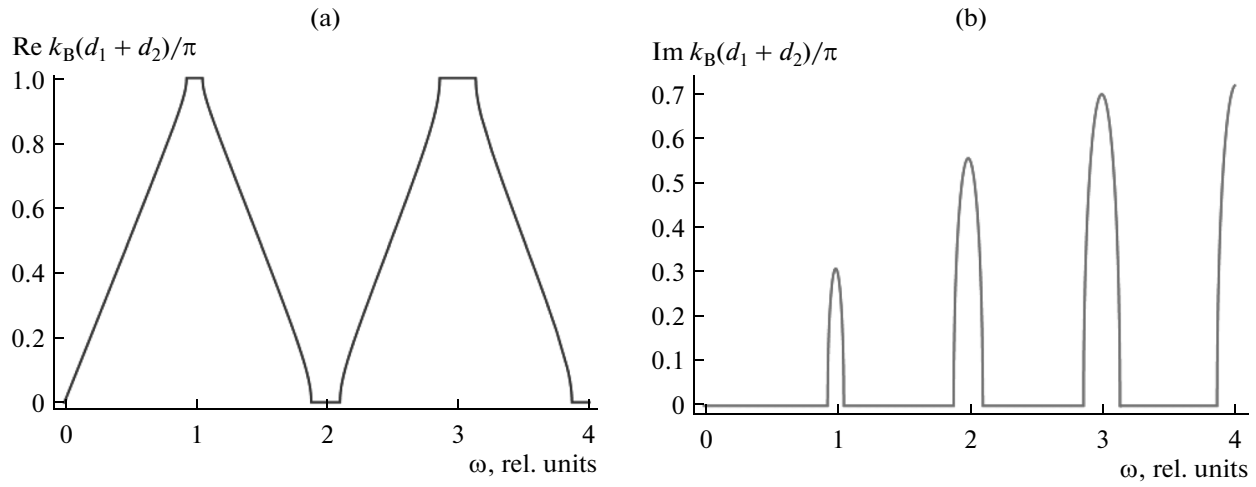

Fig. 18. Plots of (a) real and (b) imaginary parts of quantity $k_B(d_1 + d_2)$ vs. frequency.

$\mathrm{Re}\, k_B$ is π, and the imaginary part of the Bloch wave number is positive $\mathrm{Im}\, k_B > 0$ (Fig. 18).

Normally, BGs emerge in PC at frequencies for which

$$d_1 + d_2 = \frac{2\pi}{\omega} n, \tag{A1.2}$$

where n is the natural number.[9]

The electromagnetic waves at frequencies from the BG exponentially decrease upon propagation in PC and do not provide energy transfer, so that the Poynting vector $\vec{S} = \frac{c}{4\pi}[\vec{E} \times \vec{H}]$ of such waves must be zero. Hence, the electric and magnetic fields in such waves must oscillate with a phase shift of $\pi/2$. Thus, the impedance of PC ($H_z = ZE_y$) for such waves from BG is an imaginary quantity: $\mathrm{Re}\, Z_{PC} = 0$.

The group velocity in PC $v_{gr} = d\omega/dk$ strongly depends on frequency. At the boundary of BG, we have $v_{gr} \to 0$ (Fig. 18).

There is no difference between the first and second layers in the cell of the 1D PC. A 2D PC represents a homogeneous dielectric matrix that accommodates a periodic 2D grating of spatially independent perturbations. Thus, the PC properties differently depend on the permittivity of matrix (first layer) and perturbations (second layer). Such a difference leads to the absence of complete BG for both polarizations in 2D PCs. The numerical calculations show that the complete BG is formed only when the permittivity of the perturbations is less than the permittivity of the matrix [59].

[9] A PC for which $\varepsilon_1 \gg 1$ and $\varepsilon_2 \sim 1$ is an exception.

APPENDIX 2

FREQUENCY OF AMPLITUDE MODULATION

The DFB and VCSE lasers are used in optoelectronics for the transformation of electric signals into optical signals and vice versa. An important characteristic for such purposes is the frequency of amplitude modulation of signal at relatively small variations in the pump intensity that do not provide transition to the below-threshold regime of laser [24, 34].

To find the frequency of the amplitude modulation, we employ the system of equations of [25]. When radiation propagates along the normal to the layers in 1D system, the equations are represented as [25, 26]

$$\frac{\partial^2 E}{\partial x^2} - \frac{\varepsilon(x)}{c^2}\frac{\partial^2 E}{\partial t^2} = \frac{4\pi}{c^2}\frac{\partial^2 P}{\partial t^2}, \tag{A2.1}$$

$$\frac{\partial^2 P}{\partial t^2} + \frac{2}{\tau_p}\frac{\partial P}{\partial t} + \omega_{QD}^2 P = -\frac{2\omega_{QD}\left|\vec{d}\right|^2 nE}{\hbar}, \tag{A2.2}$$

$$\frac{\partial n}{\partial t} + \frac{1}{\tau_{inv}}(n - n_0) = \frac{2}{\hbar\omega_{QD}} E\frac{\partial P}{\partial t}, \tag{A2.3}$$

where E is the electric field, P is the polarization, n is the population inversion of gain medium, ω_{QD} is the QD transition frequency, $\left|\vec{d}\right|^2$ is the squared dipole moment of the transition in the gain medium, and τ_p and τ_{inv} are the characteristic relaxation times of polarization and population inversion of QDs.

The electric field and polarization can be written as

$$E = a(t)e_{\text{mode}}(x)\exp(i\omega_{\text{mode}}t) + a^*(t)e^*_{\text{mode}}(x)\exp(-i\omega_{\text{mode}}t), \quad \text{(A2.4)}$$

$$P = \sigma(t)e_{\text{mode}}(x)\exp(i\omega_{\text{mode}}t) + \sigma^*(t)e^*_{\text{mode}}(x)\exp(-i\omega_{\text{mode}}t), \quad \text{(A2.5)}$$

where $e_{\text{mode}}(x)$ is the mode of the system that satisfies equation

$$\frac{\partial^2 e_{\text{mode}}(x)}{\partial x^2} + \frac{\omega^2_{\text{mode}}}{c^2}\varepsilon(x)e_{\text{mode}}(x) = 0,$$

and ω_{mode} is the mode frequency. Variations in complex functions $a(t)$ and $\sigma(t)$ are significantly slower than variations in exponential function $\exp(i\omega_{\text{mode}}t)$. We assume that $\tau_p \gg Q/\omega_{\text{mode}}$, which is valid for the VCSE and dielectric DFB lasers. Thus, expressions (A2.1)–(A2.3) can be represented as

$$\frac{\partial a(t)}{\partial t}e_{\text{mode}}(x)\varepsilon(x) = -2\pi i\omega_{\text{mode}}e_{\text{mode}}(x)\sigma(t), \quad \text{(A2.6)}$$

$$\sigma(t) = \frac{-2\omega_{\text{QD}}|\vec{d}|^2/\hbar}{\omega^2_{\text{QD}} - \omega^2_{\text{mode}} + 2i\omega_{\text{mode}}/\tau_p}a(t)n(x,t), \quad \text{(A2.7)}$$

$$\frac{\partial n(x,t)}{\partial t} + \frac{1}{\tau_{\text{inv}}}(n(x,t) - n_0) = -\frac{2i\omega_{\text{mode}}}{\hbar\omega_{\text{QD}}}e^*_{\text{mode}}(x)e_{\text{mode}}(x)(a(t)\sigma^*(t) - a^*(t)\sigma(t)). \quad \text{(A2.8)}$$

We substitute expression (A2.7) in expressions (A2.6) and (A2.8), multiply expression (A2.6) by $a^*(t)$, and average spatial factors in expressions (A2.6) and (A2.8) with respect to the mode of the system corresponding to frequency ω_{mode}:

$$\langle f\rangle = \frac{\int e^*_{\text{mode}}(x)f(x)e_{\text{mode}}(x)dx}{\int e^*_{\text{mode}}(x)e_{\text{mode}}(x)dx}.$$

Thus, we derive equations to determine number density of photons in the cavity $S(t) = \langle\varepsilon\rangle|a(t)|^2\hbar^{-1}\omega^{-1}_{\text{mode}}$ and number density of carriers $N(t)$:

$$\frac{\partial S}{\partial t} = \frac{8\pi\omega^2_{\text{mode}}\omega_{\text{QD}}|\vec{d}|^2/(\hbar\tau_p)}{(\omega^2_{\text{QD}} - \omega^2_{\text{mode}})^2 + 4\omega^2_{\text{mode}}/\tau^2_p}\frac{SN}{\langle\varepsilon\rangle}, \quad \text{(A2.9)}$$

$$\frac{\partial N}{\partial t} + \frac{1}{\tau_{\text{inv}}}(N - N_0) = \frac{8\pi\omega^3_{\text{mode}}|\vec{d}|^2/(\hbar\tau_p)}{(\omega^2_{\text{QD}} - \omega^2_{\text{mode}})^2 + 4\omega^2_{\text{mode}}/\tau^2_p}\frac{SN}{\langle\varepsilon\rangle}. \quad \text{(A2.10)}$$

If $|\omega_{\text{QD}} - \omega_{\text{mode}}| \ll \omega_{\text{QD}}$, Eqs. (A2.9) and (A2.10) can be represented as

$$\frac{\partial S}{\partial t} = \frac{8\pi\omega_{\text{QD}}|\vec{d}|^2}{\hbar}\rho(\omega)\frac{SN}{\langle\varepsilon\rangle}, \quad \text{(A2.11)}$$

$$\frac{\partial N}{\partial t} + \frac{1}{\tau_{\text{inv}}}(N - N_0) = \frac{8\pi\omega_{\text{mode}}|\vec{d}|^2}{\hbar}\rho(\omega)\frac{SN}{\langle\varepsilon\rangle}, \quad \text{(A2.12)}$$

where $\rho(\omega) = \dfrac{1/\tau_p}{(\omega_{\text{QD}} - \omega_{\text{mode}})^2 + 1/\tau^2_p}$.

We restrict consideration to the scenario in which the frequency of cavity coincides with the frequency of the gain band ($\omega_{\text{mode}} = \omega_{\text{QD}}$) and obtain

$$\frac{\partial S}{\partial t} = \frac{2\pi\omega_{\text{QD}}\tau_p|\vec{d}|^2}{\hbar\langle\varepsilon\rangle}SN, \quad \text{(A2.13)}$$

$$\frac{\partial N}{\partial t} + \frac{1}{\tau_{\text{inv}}}(N - N_0) = \frac{2\pi\omega_{\text{QD}}\tau_p|\vec{d}|^2}{\hbar\langle\varepsilon\rangle}SN. \quad \text{(A2.14)}$$

The Maxwell–Bloch equations do not take into account spontaneous decays in the system. To take into account such processes, we supplement the equations with the corresponding terms [19, 24]:

$$\frac{dS}{dt} = g_0SN - \frac{S}{\tau_{\text{en}}} + \frac{F_{\text{mode}}}{\tau_{\text{sp}}}N, \quad \text{(A2.15)}$$

$$\frac{dN}{dt} = \frac{N_0 - N}{\tau_{\text{inv}}} - g_0SN - \frac{F_{\text{mode}} + F_{\text{rem}}}{\tau_{\text{sp}}}N, \quad \text{(A2.16)}$$

where g_0 is the gain, $\tau_{\text{en}} = Q/\omega$ is the decay time of the field energy in the cavity, τ_{sp} is the spontaneous decay time of the gain medium in free space, $F_{\text{mode}}/\tau_{\text{sp}}$ is the spontaneous decay rate to the laser mode, and $F_{\text{rem}}/\tau_{\text{sp}}$ is the spontaneous decay rate to the remaining modes.

The amplitude modulation of the signal results from the time-dependence of quantity N_0. In the presence of relatively weak amplitude modulation, the field and population inversion weakly depend on time and appear to be above the lasing threshold at any time moment, so that quantities $S(t)$, $N(t)$, and $N_0(t)$ can be represented as

$$S(t) = S^{\text{st}} + \text{Re}[s(\omega)\exp(i\omega t)], \quad \text{(A2.17)}$$

$$N(t) = N^{\text{st}} + \text{Re}[n(\omega)\exp(i\omega t)], \quad \text{(A2.18)}$$

$$N_0(t) = N_0^{\text{st}} + \text{Re}[n_0(\omega)\exp(i\omega t)], \quad \text{(A2.19)}$$

where S^{st}, N^{st}, and N_0^{st} are the stationary states of the system of equations (A2.15) and (A2.16). We substitute Eqs. (A2.17)–(A2.19) to system of equations (A2.15)

and (A2.16) and use parameters S^{st}, N^{st}, and N_0^{st} to obtain

$$\frac{s(\omega)}{n_0(\omega)} = \frac{\omega_{am}^2 \tau_{en}/\tau_{inv}}{\omega_{am}^2 - \omega^2 - i\gamma\omega}, \quad \text{(A2.20)}$$

where

$$\omega_{am}^2 = \frac{g_0 S^{st}}{\tau_{en}} + \frac{\beta F_{mode}}{\tau_{en}\tau_{sp}} \quad \text{(A2.21)}$$

is the frequency of amplitude modulation and $\beta = F_{mode}/(F_{mode} + F_{rem})$ is the ratio of the spontaneous decay rate to the laser mode to the spontaneous decay rate to the remaining modes.

REFERENCES

1. X. Jiang and C. M. Soukoulis, Phys. Rev. B **59**, 6159 (1999).
2. S. Strauf, K. Hennessy, M. T. Rakher, et al., Phys. Rev. Lett. **96**, 127404 (2006).
3. M. Imada, A. Chutinan, S. Noda, and M. Mochizuki, Phys. Rev. B **65**, 195306 (2002).
4. M. Notomi, H. Suzuki, T. Tamamura, and K. Edagawa, Phys. Rev. Lett. **92**, 123906 (2004).
5. N. I. Zheludev, S. L. Prosvirnin, N. Papasimakis, and V. A. Fedotov, Nature Photon **2**, 351 (2008).
6. Y.-W. Huang, W. T. Chen, P. C. Wu, et al., Sci. Rep. **3**, 1237 (2013).
7. J. Y. Suh, C. H. Kim, W. Zhou, et al., Nano Lett. **12**, 5769 (2012).
8. F. Beijnum, P. J. Veldhoven, E. J. Geluk, et al., Phys. Rev. Lett. **110**, 206802 (2013).
9. W. Zhou, M. Dridi, J. Y. Suh, et al., Nat. Nanotechnol. **8**, 506 (2013).
10. I. E. Protsenko, A. V. Uskov, O. A. Zaimidoroga, et al., Phys. Rev. A **71**, 063812 (2005).
11. I. E. Protsenko, A. V. Uskov, K. E. Krotova, and E. P. O'Reilly, J. Phys.: Conf. Ser. **107**, 012010 (2008).
12. N. N. Ledentsov and D. A. Lott, Usp. Fiz. Nauk **181**, 884 (2011).
13. K. Iga, IEEE J. Sel. Top. Quantum Electron. **6**, 1201 (2000).
14. C. J. Chang-Hasnain, IEEE J. Sel. Top. Quantum Electron. **6**, 978 (2000).
15. G. Steinle, H. Riechert, and A. Y. Egorov, Electron. Lett. **37**, 93 (2001).
16. W. Yuen, G. S. Li, R. F. Nabiev, et al., Electron. Lett. **36**, 1121 (2000).
17. F. Koyama, J. Lightwave Technol. **24**, 4502 (2006).
18. J. A. Lott, V. A. Shchukin, N. N. Ledentsov, et al., Electron. Lett. **47**, 717 (2011).
19. L. A. Coldren and S. W. Corzine, *Diode Lasers and Photonic Integrated Circuits* (Wiley, New York, 1995).
20. A. A. Zyablovskii, A. V. Dorofeenko, A. A. Pukhov, A. P. Vinogradov, E. S. Andrianov, A. B. Granovskii, and A. A. Lisyanskii, J. Commun. Technol. Electron. **60**, 87 (2015).
21. H. J. Unold, S. W. Z. Mahmoud, R. Jager, et al., IEEE Photonics Technol. Lett. **12**, 939 (2000).
22. C. Degen, W. Elsaber, and I. Fischer, Opt. Express **5** (3), 38 (1999).
23. P. V. Mena, J. J. Morikuni, S. M. Kang, et al., J. Lightwave Technol. **17**, 865 (1999).
24. D. Englund, H. Altug, B. Ellis, and J. Vuckovic, Laser Phot. Rev. **2**, 264 (2008).
25. G. L. Lamb, Rev. Mod. Phys. **43** (2), 99 (1971).
26. A. V. Dorofeenko, A. A. Zyablovskii, A. A. Pukhov, et al., Usp. Fiz. Nauk **182**, 1157 (2012).
27. A. A. Zyablovskii, A. V. Dorofeenko, A. A. Pukhov, and A. P. Vinogradov, J. Commun. Technol. Electron. **56**, 1139 (2011).
28. A. H. Schokker and A. F. Koenderink, Phys. Rev. B **90**, 155452 (2014).
29. A. A. Zyablovsky, A. V. Dorofeenko, A. P. Vinogradov, and A. A. Pukhov, Photonics Nanostruct. Fundam. Appl. **9**, 398 (2011).
30. S. M. Rytov, Zh. Eksp. Teor. Fiz. **29**, 605 (1955).
31. A. P. Vinogradov, Y. E. Lozovik, A. M. Merzlikin, et al., Phys. Rev. B. **80**, 235106 (2009).
32. S.-L. Chua, Y. Chong, A. D. Stone, et al., Opt. Express **19**, 1539 (2011).
33. C. A. Balanis, *Antenna Theory – Analysis and Design*, 3rd Ed. (Wiley-Intersci., New York, 2005).
34. A. Mutig and D. Bimberg, Advances Opt. Technol. **2011**, 290508 (2011).
35. H. Altug, D. Englund, and J. Vuckovic, Nature Phys. **2**, 484 (2006).
36. D. J. Bergman and M. I. Stockman, Phys. Rev. Lett. **90**, 027402 (2003).
37. M. A. Noginov, G. Zhu, A. M. Belgrave, et al., Nature **460**, 1110 (2009).
38. Y.-J. Lu, J. Kim, H.-Y. Chen, et al., Science **337**, 450 (2012).
39. A. A. Kolokolov and G. V. Skrotskii, Usp. Fiz. Nauk **162** (12), 165 (1992).
40. M. I. Stockman, J. Opt. **12**, 024004 (2010).
41. X. Meng, J. Liu, A. V. Kildishev, and V. M. Shalaev, Laser Phot. Rev. **8**, 896 (2014).
42. M. T. Hill, M. Marell, E. S. P. Leong, et al., Opt. Express **17**, 11107 (2009).
43. T. Pickering, J. M. Hamm, A. F. Page, et al., Nat. Commun. **5**, 4972 (2014).
44. P. W. Milonni, *Fast Light, Slow Light and Left-Handed Light* (IOP Publishing, London, 2005).
45. V. M. Agranovich, *Surface Polaritons: Electromagnetic Waves on Surfaces and Interfaces,* Ed. by V.M. Agranovich and D.L. Mills (Nauka, Moscow, 1985) [in Russian].

46. S. A. Ramakrishna, J. B. Pendry, M. C. K. Wiltshire, and W. J. Stewart, J. Mod. Opt. **50**, 1419 (2003).

47. A. N. Lagar'kov, A. K. Sarychev, V. N. Kisel', and G. Tartakovskii, Usp. Fiz. Nauk **179**, 1018 (2009).

48. A. K. Sarychev, A. A. Pukhov, and G. Tartakovsky, PIERS Online **3**, 1264 (2007).

49. A. V. Dorofeenko, A. A. Zyablovsky, A. P. Vinogradov, et al., Opt. Express **21**, 14539 (2013).

50. E. S. Andrianov, A. A. Pukhov, A. V. Dorofeenko, et al., Phys. Rev. B **85**, 165419 (2012).

51. A. A. Zyablovsky, A. V. Dorofeenko, A. P. Vinogradov, et al., AIP Conf. Proc. **1475**, 185 (2012).

52. R. H. Dicke, Phys. Rev. **93**, 99 (1954).

53. E. S. Andrianov, A. A. Pukhov, A. V. Dorofeenko, et al., Opt. Express **19**, 24849 (2011).

54. A. N. Oraevskii, Kvant. Elektronika **29** (2), 37 (1999).

55. S. Solimeno, B. Crosignani, and P. Di Porto, *Guiding, Diffraction and Confinement of Optical Radiation* (Academic, Orlando, 1986; Mir, Moscow, 1989).

56. Ya. I. Khanin, *Principles of Laser Dynamics* (Nauka, Moscow, 1999) [in Russian].

57. R. H. Pantell and H. E. Puthoff, *Fundamentals of Quantum Electronics* (Wiley, New York, 1969; Mir, Moscow, 1972).

58. M. O. Skalli and M. S. Zubairi, *Quantum Optics* (Fizmatlit, Moscow, 2003) [in Russian].

59. J. D. Joannopoulos, P. R. Villeneuve, and S. Fan, Nature **386**, 143 (1997).

Translated by A. Chikishev